TECHNISCHE UNIVERSITÄT WIEN

MASTER THESIS

Influencing the binder properties in tungsten heavy alloys (WHA)

Institut für chemische Technologien und Analytik - TU Wien
Getreidemarkt 9/164-CT
1060 Wien

under the supervision of

Ao.Univ.Prof. Dipl.-Ing. Dr.techn. Christian EDTMAIER

Lena Maria Dorner, BSc.
01425814

WIEN, 06.03.2023
Ort, Datum

[redacted]
Unterschrift

Die approbierte gedruckte Originalversion dieser Diplomarbeit ist an der TU Wien Bibliothek verfügbar
The approved original version of this thesis is available in print at TU Wien Bibliothek.
TU Bibliothek Your knowledge hub WIEN

Eidesstattliche Erklärung

Ich erkläre an Eides statt, dass die vorliegende Arbeit nach den anerkannten Grundsätzen für wissenschaftliche Abhandlungen von mir selbstständig erstellt wurde. Alle verwendeten Hilfsmittel, insbesondere die zugrunde gelegte Literatur, sind in dieser Arbeit genannt und aufgelistet. Die aus den Quellen wörtlich entnommenen Stellen, sind als solche kenntlich gemacht. Das Thema dieser Arbeit wurde von mir bisher weder im In- noch Ausland einer Beurteiler*in zur Begutachtung in irgendeiner Form als Prüfungsarbeit vorgelegt. Diese Arbeit stimmt mit der von den Begutachter*innen beurteilten Arbeit überein.

WIEN, 06.03.2023
Ort, Datum

[redacted]
Unterschrift

Die approbierte gedruckte Originalversion dieser Diplomarbeit ist an der TU Wien Bibliothek verfügbar
The approved original version of this thesis is available in print at TU Wien Bibliothek.
TU Bibliothek Your knowledge hub WIEN

Abstract

Tungsten heavy metal composites (WHA) have been in development for a long time as the high density and the high melting point of tungsten make these composites interesting for high-temperature applications. In this work, materials with Ni/Fe, Ni/Fe/Mo and Ni/Cu binder were investigated. These materials are already well studied, however, properties, such as specific electrical resistivity, thermal conductivity, saturation magnetization and Young's modulus should be further improved. Moreover, as seen in [1], thermal and electrical conductivity do not fit together, which is why further investigations on this relationship was done in this thesis.

The aforementioned properties may be influenced in two ways. One attempt is to address the interface between tungsten particles and the matrix and the other attempt is to influence the binder itself. This was executed with different heat treatment schemes. The binder samples were produced with powder hot extrusion. The microstructures were analysed with scanning electron microscopy (SEM) and X-ray diffraction (XRD). In addition, tensile tests were carried out to detect possible segregation effects at the grain boundaries.
Furthermore, the validity of the Wiedemann-Franz law was tested on binder materials. For this purpose, the electrical conductivity of the binder materials was measured between 4.2 K and room temperature.

The properties of WHAs were mainly changed by annealing the samples at temperatures from 1000 °C and annealing times of 20 h or 120 h. A correlation between the thermal and electrical conductivity is hardly discernible in WHAs. Kinetic effects are particularly effective with the material IT180. Hot extrusion made it possible to produce non-porous binder materials. SEM images of binder materials show that further heat treatment causes tungsten to dissolve in the binder. No major influence of different heat treatments can be seen in the binder materials. The Wiedemann-Franz law does not seem to apply to this binder materials.

Die approbierte gedruckte Originalversion dieser Diplomarbeit ist an der TU Wien Bibliothek verfügbar
The approved original version of this thesis is available in print at TU Wien Bibliothek.
TU Bibliothek Your knowledge hub WIEN

Kurzfassung

Wolfram-Schwermetall-Verbundwerkstoffe (WHA) sind seit langem im Einsatz, da die hohe Dichte und der hohe Schmelzpunkt von Wolfram diese Verbundwerkstoffe für Hochtemperaturanwendungen interessant machen. In dieser Arbeit wurden Materialien mit Ni/Fe, Ni/Fe/Mo und Ni/Cu als Binder untersucht. Diese Werkstoffe sind bereits gut erforscht, jedoch sollten Eigenschaften wie spezifischer elektrischer Widerstand, Wärmeleitfähigkeit, Sättigungsmagnetisierung und Elastizitätsmodul weiter verbessert werden. Außerdem passen, wie [1] zeigt, Wärme- und elektrische Leitfähigkeit nicht zusammen, weshalb in dieser Arbeit weitere Untersuchungen durchgeführt wurden, um diesen Zusammenhang zu prüfen.

Die zuvor genannten Eigenschaften könnten auf zwei Arten beeinflusst werden. Zum einen wird versucht, die Grenzfläche zwischen Wolframpartikeln und der Matrix zu verändern, zum anderen wird versucht, den Binder selbst zu beeinflussen. Dies wurde mit verschiedenen Wärmebehandlungsverfahren durchgeführt. Die Binderproben wurden durch Strangpressen hergestellt. Die Mikrostrukturen wurden mit Rasterelektronenmikroskopie (SEM) und Röntgenbeugung (XRD) analysiert. Darüber hinaus wurden Zugversuche durchgeführt, um mögliche Entmischungseffekte an den Korngrenzen festzustellen.
Darüber hinaus wurde die Gültigkeit des Wiedemann-Franz-Gesetzes an den Binderproben geprüft. Zu diesem Zweck wurde die elektrische Leitfähigkeit zwischen 4.2 K und Raumtemperatur gemessen.

Die Eigenschaften von WHAs wurden vor allem durch Wärmebehandlungen der Proben bei Temperaturen ab 1000 und Glühzeiten von 20 h oder 120 h verändert. Eine Korrelation zwischen der thermischen und der elektrischen Leitfähigkeit ist bei WHAs kaum zu erkennen. Kinetische Effekte sind bei dem Werkstoff IT180 besonders wirksam. Durch Strangpressen konnten porenfreie Binder hergestellt werden. REM-Aufnahmen davon zeigen, dass eine weitere Wärmebehandlung dazu führt, dass sich das Wolfram im Binder auflöst aber es war kein wesentlicher Einfluss unterschiedlicher Wärmebehandlungen zu erkennen. Das Wiedemann-Franz-Gesetz scheint für diese Bindermaterialien nur eingeschränkt zu gelten.

Die approbierte gedruckte Originalversion dieser Diplomarbeit ist an der TU Wien Bibliothek verfügbar
The approved original version of this thesis is available in print at TU Wien Bibliothek.
TU Bibliothek Your knowledge hub WIEN

Danksagung

Ganz besonderen Dank möchte ich an Ao.Univ.Prof.Dipl.-Ing.Dr.techn. Christian Edtmaier aussprechen, für seine Geduld und aufmunternden Worte. Er stand immer für offene Fragen bereit und konnte mir bei Problemen weiterhelfen.

Weiters möchte ich auch meinen Projektpartnern für die gute Zusammenarbeit und Finanzierung des Projekts bedanken. Durch die zahlreichen Meetings konnten sie mir immer neuen Input geben. Außerdem standen sie mir bei Problemen und Fragen immer zur Seite. Vielen Dank für die Erfahrungen.

Ich möchte hiermit auch meinen Kollegen aus der Werkstatt danken. Trotz meiner nicht ganz leicht bearbeitbaren Proben, nahmen sie jede Herausforderung an und reparierten wochenlang das für diese Arbeit notwendige Messgerät.

Besonderer Dank gilt auch allen meinen Kollegen für die zahlreichen Ratschläge und Hilfestellungen im Zuge dieser Arbeit. Danke für die unvergesslich schöne Zeit, auch außerhalb der Arbeit. Besonderes bedanken möchte ich mich dabei an Peter Nahringbauer, der mich im gesamten Masterstudium begleitet hat und mir auch während dieser Arbeit immer zur Seite gestanden ist.

Zuletzt möchte ich natürlich auch meiner Familie und Freunde danken für die Geduld mit mir auf diesem Weg. Vor allem möchte ich meinen Eltern für die geistige und finanzielle Unterstützung danken, ohne sie wäre das alles nicht möglich gewesen.

Die approbierte gedruckte Originalversion dieser Diplomarbeit ist an der TU Wien Bibliothek verfügbar
The approved original version of this thesis is available in print at TU Wien Bibliothek.
TU Bibliothek Your knowledge hub WIEN

Contents

Die approbierte gedruckte Originalversion dieser Diplomarbeit ist an der TU Wien Bibliothek verfügbar
The approved original version of this thesis is available in print at TU Wien Bibliothek.
TU Bibliothek Your knowledge hub WIEN

Die approbierte gedruckte Originalversion dieser Diplomarbeit ist an der TU Wien Bibliothek verfügbar
The approved original version of this thesis is available in print at TU Wien Bibliothek.

1 Introduction

1.1 Tungsten heavy alloys

What makes tungsten heavy alloys so interesting to work with, is its high density of up to 19 g/cm^3. This high density derives from the main constituent tungsten, which has a density of 19.3 g/cm^3. Tungsten rates among the elements with the highest density and from all metals, tungsten is the one element with the highest melting point and can therefore be used in high temperature treatments. Furthermore, tungsten has a very low coefficient of thermal expansion, a high dimensional stability and is quite resilient. Compared to other high-density elements, tungsten has a wide spectrum of applications in industries. Due to the high tungsten content of at least 90 % in WHAs, tungsten is mainly responsible for the excellent properties of WHAs.

WHAs have a broad spectrum of applications. They range from medical technology to aerospace industries. Considering the good ability of WHAs at shielding gamma and X-rays, they are used as radiation shields. This can be applied, for example, in medical technology, more precisely in radiotherapy. The collimator not only shields the radiation, but also ensures that the radiation reaches the desired location with pinpoint accuracy to cause as little damage as possible to healthy tissue. WHAs are also used as vibration dampers or in munitions that use only kinetic energy to hit their target. Furthermore, they are used in watches as oscillating weights [2].

The mechanical properties of WHAs are not considered to be substantial for applications where the high density of WHAs plays an important role [3]. This might occur with radiation protection applications where strength and ductility are not very important. Other applications, however, require a material with high strength and ductility. WHAs can also be used for these applications, when previously processed. With heat treatments, the mechanical properties can be improved. This is for example necessary when producing kinetic energy penetrators [2].

WHA is the definition of materials with a high tungsten content and at least two binder materials that form a biphasic microstructure in which the tungsten particles are body-centered cubic and the matrix of the binder materials are face-centered cubic. However, it is important to note, that tungsten is also partially dissolved in the binder. The most common binder materials are iron, nickel, copper and molybdenum, which are also investigated in this thesis. Cobalt was a

Die approbierte gedruckte Originalversion dieser Diplomarbeit ist an der TU Wien Bibliothek verfügbar
The approved original version of this thesis is available in print at TU Wien Bibliothek.
TU Bibliothek Your knowledge hub WIEN

popular binder material as well, however, due to its carcinogenicity, cobalt is to be avoided [4].

1.2 Production of WHAs

The production process essentially consists of 5 steps: powder production, mixing two or more powders, pressing, sintering and post-sintering.
Tungsten powders are generally produced by oxide powder reduction. Nickel and iron powders can be produced by the decomposition of metal carbonyl compounds [3].

The powders used are mixed until homogeneous. The powder mixture is then pressed in its shape. This is done with an uniaxial die press or isostatic press, for example [5]. The outcome is the so-called green part. It is compacted, but still porous and fragile.

To densify the material, the green part must undergo further heat treatment. This step is what is meant by the term sintering and is carried out at a temperature below the melting point of the main component.
With this approach, the pores should be reduced with grain growth and structural defects are degraded. With sintering, the energy content of a dispersed system is reduced. The driving force of sintering is the decrease in free enthalpy between the initial and final state. There are two different ways for sintering: solid-state and liquid-phase sintering. The samples used in this thesis are provided by Plansee Composite Material GmbH, Germany and were produced by liquid-phase sintering. A distinction can be made between 2 types of liquid-phase sintering. One way is sintering in equilibrium where the composition and quantity do not change, the liquid phase is stationary. Strong compaction is achieved in the process. The other way is sintering in a thermodynamic disequilibrium where solid solution formation is built and an intermediate liquid phase exists. In this case, the low-melting component in the matrix has good solubility and swelling occurs. A very important factor for sintering is wetting. If the wetting factor is high, the melt can penetrate into the press contact and enclose particles from all sides. This is how the material can shrink. The driving force of sintering is the attraction of solid particles, the hydrostatic pressure on pores and the movement of particles against the viscosity of the melt [6].

Die approbierte gedruckte Originalversion dieser Diplomarbeit ist an der TU Wien Bibliothek verfügbar
The approved original version of this thesis is available in print at TU Wien Bibliothek.
TU Bibliothek Your knowledge hub WIEN

1.3 WHA materials

Figure 1 shows the typical microstructure of a WHA with the main fraction of tungsten (grey phase) and a smaller fraction of binder in between (dark phase).

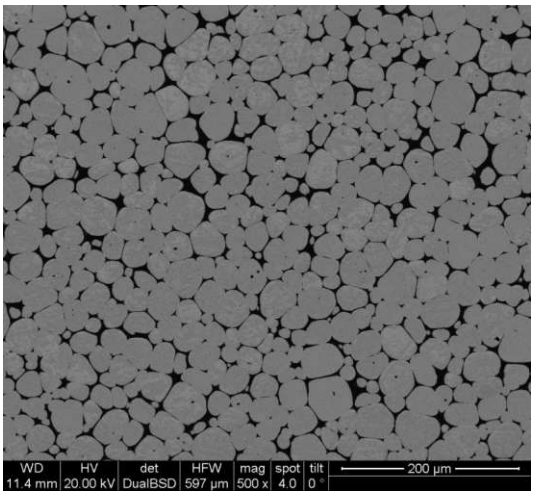

Fig. 1: Microstructure of a W-Ni-Fe WHA

Plansee Composite Material GmbH, Germany produces different types of WHAs, e.g. those with the brand names DENSIMET® and INERMET® , the former having a weakly ferromagnetic Fe-Ni binder, the latter a paramagnetic Ni-Cu one. In both WHA families, the different materials are abbreviated as Dxxx, or ITxxx, where xxx is a number representing the density. E.g. D176 is a DENSIMET® material of density 17.6 g/cm^3. Commercially, D170, D176, D180, D185, D188 and IT170, IT176 and IT180 are offered. Among the DENSIMET®-Materials there is another special feature, namely one with a Ni-Fe-Mo binder, D2M. The most important physical and thermophysical properties can be found in [1], but the most relevant properties for this work, i.e. thermal conductivity, electrical resistivity, saturation magnetization, tensile strength and Young's Modulus are summarised in table 1 for the materials of interest D180, D185, D2M and IT180. Since the relationship between electrical and thermal conductivity is also of interest in this work, the measured electrical resistance [1] was converted into a thermal conductivity in table 1 using the Wiedemann-Franz law (see also chapter 3.3.8) in order to be able to compare this with the measured one. As can be seen, there is a significant discrepancy between the two values.

Die approbierte gedruckte Originalversion dieser Diplomarbeit ist an der TU Wien Bibliothek verfügbar
The approved original version of this thesis is available in print at TU Wien Bibliothek.
TU Bibliothek Your knowledge hub WIEN

Tab. 1: Values of specific electrical resistivity, thermal conductivity, saturation magnetization and Young's modulus of materials D185, D180, D2M and IT180, as stated in [1], [7]

	D185	**D180**	**D2M**	**IT180**
specific electrical resistivity ($\mu\Omega$m)	0.106	0.106	0.163	0.116
thermal conductivity (W/m*K)	85.77	85.77	60	108.15
thermal conductivity calculated (W/m*K)	67	67	44	61
Saturation magnetization (μT*m^3/kg)	3.1	5.1	5.7	-
Young's modulus (GPa)	385	380	-	360
Tensile strength (MPa)	800	800	-	685

Die approbierte gedruckte Originalversion dieser Diplomarbeit ist an der TU Wien Bibliothek verfügbar
The approved original version of this thesis is available in print at TU Wien Bibliothek.
TU Bibliothek Your knowledge hub WIEN

2 Problem definition

To improve the the thermal conductivity, specific electrical resistivity, saturation magnetization and Young's modulus even further, two parameters in particular may be influenced. Firstly, the interface between tungsten particles and the matrix could be influenced. Secondly, the binder itself could be influenced. Since dissolved elements play an important role in the degradation of properties with regard to conductivity, attempts should be made to precipitate these dissolved elements from the matrix by means of suitable heat treatment schemes in order to improve the properties of WHAs, such as electrical resistivity, thermal conductivity, saturation magnetization and Young's modulus. The changes of these 4 properties should be measured as a function of heat treatments, temperature and time ("kinetics").

To learn about differences in the matrix after different heat treatments, the fracture surfaces of samples, pre-annealed at different temperatures, can be observed. Therefore, tensile tests should be performed, that also give information about the yield strength, tensile strength and ductility of a material. With this method also Young's modulus, tensile strength and elongation can be measured. The only requirement is, that the material is not too brittle, like ceramics or hard metals. Therefore it is well suited for heavy metals. Especially WHAs are known for its high ductility. Elongation of heavy metals reaches up to 30 %, considering that elongation of pure tungsten is only 1 to 3 %, [8]. This is due to the strength of the interphase between tungsten and the binder. The fracture surface may also provide information on the fracture behavior and the fracture mechanism [8], it is thus of interest to evaluate the influence of heat treatment on the fracture behaviour.

Furthermore, it is interesting to investigate the binder alone, i.e. without the main component tungsten, in a more targeted way. For this purpose, samples with the main components nickel and iron as well as with increasing tungsten content should be produced in order to determine the changes in the properties as a function of the dissolved or precipitated tungsten after heat treatments ("binder material"). It is investigated, that e.g. dissolved tungsten lowers the saturation magnetization of nickel-iron samples [3].

As shown in [3], producing those binder materials is challenging. To get rid of pores within the material, two attempts will be made in this thesis, where one is sintering and the other is hot extrusion.

Die approbierte gedruckte Originalversion dieser Diplomarbeit ist an der TU Wien Bibliothek verfügbar
The approved original version of this thesis is available in print at TU Wien Bibliothek.
TU Bibliothek Your knowledge hub WIEN

After pressing metal powders to a green part, pores might still remain in the sample. Although, pores might be desired for some materials, getting rid of pores is necessary for many materials, particularly for this binder materials to maintain the high density of the material and to enhance the properties of the specimen, hence, to be even able to measure them correctly, e.g. thermal conductivity. Pressing is not the only process, pores occur. Additionally, pores may be formed during the sintering process. In these pores, the gas from the sintering atmosphere, usually hydrogen or argon, is trapped and needs to diffuse out of the material [3].

With the method of hot extrusion, the binder materials can be densified through high pressure. The application of extrusion to porous metals with the aim of densifying them has already been described in several publications [9] [10]. Hot extrusion is mainly used and known for aluminum alloys. Previous works have shown, that extrusion can also be applied to WHAs [11], [12]. In these cases, extrusion was used to improve the susceptibility to adiabatic shear band.

As displayed in table 1, the values for thermal and electrical conductivity do not quite match. The Wiedemann Franz law assumes a direct proportionality of the thermal conductivity with the electrical conductivity, which is the reciprocal of the specific electrical resistivity, [13]. Therefore, a more detailed investigation should also be carried out here.

Die approbierte gedruckte Originalversion dieser Diplomarbeit ist an der TU Wien Bibliothek verfügbar
The approved original version of this thesis is available in print at TU Wien Bibliothek.
TU Bibliothek Your knowledge hub WIEN

3 Experimental

3.1 Kinetics

3.1.1 Material

4 different materials of the brands DENSIMET® and INERMET® were provided by Plansee Composite Materials GmbH. The three DENSIMET® materials are D185, D180 and D2M, the INERMET® material is IT180. The main component is tungsten and takes up 90 to 97 wt%. The binder materials are nickel, iron, molybdenum and copper.

3.1.2 Density

The density from the sintered binder materials was determined by using the Archimedes' method. This was accomplished by measuring the weight of the materials in air and in water, separately. By knowing the density of water, the formula 1 was used to determine the density.

$$\rho = \frac{F_{G,1}}{F_{G,1} - F_{G,2}} \cdot \rho_2 \tag{1}$$

The subscript 1 stands for the less dense medium, whereas the subscript 2 is for the denser medium.

3.1.3 Heat treatments on bar samples

Two types of heat treatments were performed. One type was non-consecutive heat treatments, where a new sample was used for every annealing temperature. The other type was consecutive heat treatments, where one sample was used for several heat treatments at different temperatures.

For non-consecutive heat treatments, 3 heat treatments were made at the same temperature and time. In the first run, one sample of each material was annealed at one temperature for a specific isothermal time. The set temperatures started at 800 °C and went up to 1300 °C in steps of hundreds. The isothermal times were either set to 2 h, 20 h or 120 h, see figure 2. The annealing itself happened in a tube furnace, where the samples were introduced in a steel boat. All samples were introduced in the preheated furnace only when it had already reached the desired set temperature. In the cooling zone, integrated in the furnace, the samples could cool down to room temperature after the heat treatment. Argon gas was flowing through the furnace during the entire heat treatment. Unless otherwise stated,

Die approbierte gedruckte Originalversion dieser Diplomarbeit ist an der TU Wien Bibliothek verfügbar
The approved original version of this thesis is available in print at TU Wien Bibliothek.
TU Bibliothek Your knowledge hub WIEN

argon gas was used for all heat treatments described in this thesis.
For particular temperatures and annealing times, a second run was performed with unused samples, to prove the reproducibility.

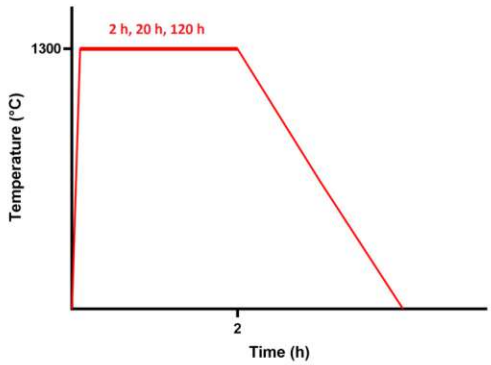

Fig. 2: Temperature profile of non-consecutive heat treatment of WHAs

For consecutive heat treatments, two experiments were executed. In the first experiment, the samples were pre-annealed at 1200 °C for 120 h, which was then considered the new as-sintered state. The samples were then annealed at 1200 °C for 2 h and after cooling down, again annealed for 2 h, but this time at 1000 °C, figure 3a.
For the second consecutive experiment, the samples were pre-annealed at 1300 °C for 120 h, which was then considered the new as-sintered state. After this, the samples were again annealed at 1300 °C for 2 h, at 800 °C for 2 h and finally at 1000 °C for 2 h, see figure 3b. Between each annealing step, the samples were cooled down and 4 properties were measured. Those properties are the specific electrical resistivity, thermal conductivity, saturation magnetization and Young's modulus, see section 3.3.

Die approbierte gedruckte Originalversion dieser Diplomarbeit ist an der TU Wien Bibliothek verfügbar
The approved original version of this thesis is available in print at TU Wien Bibliothek.

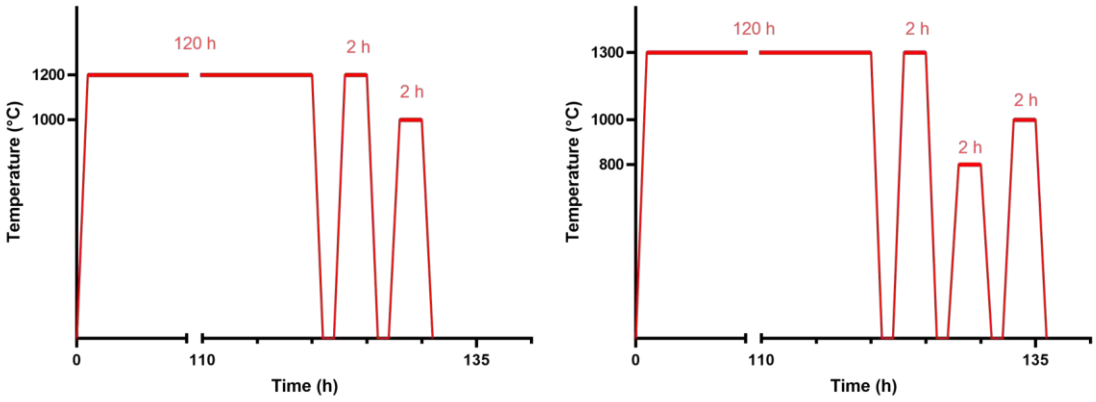

(a) 1. experiment **(b)** 2. experiment

Fig. 3: Temperature profile of consecutive heat treatments of WHAs

3.1.4 Tensile tests on dumbbell samples

According to DIN 50125 [14], the sample geometry must be a proportional rod. The exact dimensions are given in the schematic drawing in figure 4.

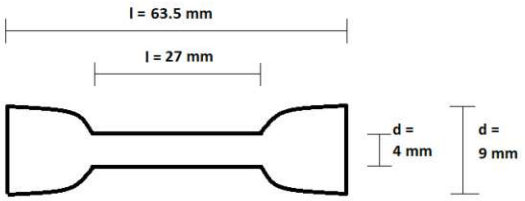

Fig. 4: Dumbbell sample for tensile tests, where l = length and d = diameter

In this thesis, only the two materials D180 and IT180 were used for tensile testing. 9 samples of each material in total were tested, see table 2. From these 9 samples, 3 were measured in the as-sintered state. 3 other samples were annealed at 1100 °C for 2 hours before performing the tensile test and 3 more samples were annealed for 2 h at 1300 °C before tensile testing. The annealing procedure was exactly the same as described in section 3.1.3 for non-consecutive heat treatments. The tensile testing was performed on a universal testing machine (Zwick 1474, Zwick Roell) and was executed via a video extensometer. The crosshead speed was 5 mm/min. All measurements took place at room temperature. The stress-strain curves could then be documented and used to determine the tensile strength and strain. Furthermore, the fracture surfaces of all samples were analysed using scanning electron microscopy.

Die approbierte gedruckte Originalversion dieser Diplomarbeit ist an der TU Wien Bibliothek verfügbar
The approved original version of this thesis is available in print at TU Wien Bibliothek.

Tab. 2: Samples used for tensile tests

Material	as-sintered	1100 °C	1300 °C
D180	sample 1	sample 4	sample 7
	sample 2	sample 5	sample 8
	sample 3	sample 6	sample 9
IT180	sample 1	sample 4	sample 7
	sample 2	sample 5	sample 8
	sample 3	sample 6	sample 9

3.2 Binder material

3.2.1 Material

The binder material was produced analogously to material D180. The iron/nickel ratio was exactly the same as in D180 and remained constant in all binder samples. The only component that changed was the tungsten content. In total 4 samples were prepared with tungsten contents of 0, 10, 20 and 30 % each.
All powders were provided by Plansee Composite Materials GmbH. The tungsten powder had a grain size of 4 µm. Unfortunately, the grain sizes of the other powders are not known. Nickel, iron and tungsten powders were mixed in the Turbula tumble mixer for 45 min each, pressed and sintered afterward.

3.2.2 Sintering

Two attempts were made to produce dense samples. The first one was different sintering processes.
First experiments included sintering processes at 1400 °C for 2 h in a hydrogen atmosphere.
Another experiment was executed in a sinter-HIP (FCT Systeme GmbH). The samples were heated up to 1400 °C with a heating rate of 10 K/min and then held for 20 min. The gas pressure was 60 bar and the atmosphere was argon gas. The temperature was then changed to 1250 °C for another experiment.
For hot extrusion experiments, described in the following, section 3.2.3, pressed powders were heated up to 1000 °C and held at this temperature for 2 h in an atmosphere of hydrogen gas. Subsequently, the atmosphere was switched to argon gas and the samples were cooled down.

Die approbierte gedruckte Originalversion dieser Diplomarbeit ist an der TU Wien Bibliothek verfügbar
The approved original version of this thesis is available in print at TU Wien Bibliothek.
TU Bibliothek Your knowledge hub WIEN

3.2.3 Hot extrusion

The second attempt for achieving non-porous binder materials was shear forces and sintering powder hot extrusion.
Binder samples pre-sintered at 1460 °C for 5 h in H_2 atmosphere were transferred into an iron capsule. After the capsule was gas-tight welded, it was put in another furnace. The capsule was pre-heated at 1200 °C for 20 min. From the furnace, the capsule was directly introduced into the extrusion press from V. Jessernigg Urban, as shown in figure 5.

Fig. 5: Hot extrusion press at TU Wien

The result was a rod with a thickness of around 12 mm and a length of about 250 mm.
Right after the extrusion, the steel capsules were still covering the samples, which is why the steel had to be removed by turning before further processing. The sample was cut and brought to a diameter of 8 mm for further processing, see figure 6.

Die approbierte gedruckte Originalversion dieser Diplomarbeit ist an der TU Wien Bibliothek verfügbar
The approved original version of this thesis is available in print at TU Wien Bibliothek.

Fig. 6: Binder material after extrusion with and without steel coat

3.2.4 Heat treatments

The heat treatments for binder materials were executed as described in section 3.1.3. For the binder materials only consecutive heat treatments were implemented, due to the limited value of hot extruded material. Before, the binder materials has been firstly annealed at 1250 °C for 72 h to ensure that all alloying elements are dissolved, as elemental powders were used. After that, the binder materials were annealed at 1300 °C, 1000 °C, and 800 °C for 2 h each. As described in section 3.1.3, between every heat treatment, the binder samples were cooled down and the specific electrical resistivity, thermal conductivity, saturation magnetization and the Young's modulus were measured.

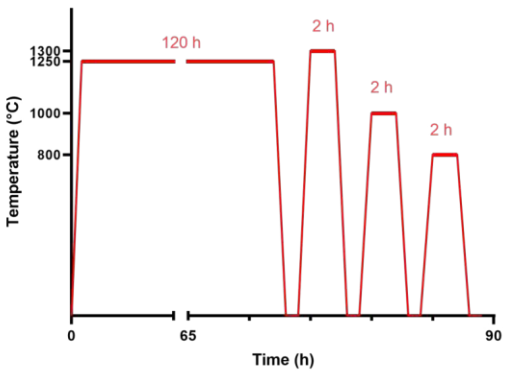

Fig. 7: Temperature profile of consecutive heat treatments of binder material

3.3 Characterization

After the heat treatments, four properties, i.e. thermal conductivity, specific electrical resistivity, saturation magnetization and Young's modulus were measured.

Die approbierte gedruckte Originalversion dieser Diplomarbeit ist an der TU Wien Bibliothek verfügbar
The approved original version of this thesis is available in print at TU Wien Bibliothek.

Each property was measured four times on each sample. The uncertainty of measurements often lies in the sample geometry. Every sample had to have at least 6 mm width and 30 mm length. To be able to compare the samples and to exclude the uncertainty of measurements as good as possible, every sample has to have the exact same geometry. For bar samples the geometry was exactly 6 x 6 x 30 mm. Binder materials had a diameter of 8 mm and a length of 30 mm.

3.3.1 Thermal conductivity

The thermal conductivity was measured on a device, manufactured at TU Wien, using the direct thermal conductivity method. For this purpose, the sample is clamped between two copper plates. The sample is switched in series with a reference sample. One side is cooled to 5 °C and the other heated to 95 °C. The temperature is measured at different positions on both samples when the equilibrium has been reached. With that information, the temperature gradient can be calculated. The observational error with this device is a maximum of 3 - 5 %.

3.3.2 Specific electrical resistivity

The specific electrical resistivity was measured on a device, engineered at TU Wien. The measured sample was placed horizontally on the device. By turning a switch to ‘close‘, four electrodes in total move towards the sample. Right after all four electrodes are touching the sample, the electrical resistivity can be read off the device. The request on the sample is the right geometry and a temperature of exactly 20 °C.

3.3.3 Saturation magnetization

The saturation magnetization is the maximum of the magnetization, that is reached, when an increasing external magnetic field cannot affect the magnetization of the material any further. Due to the ferromagnetic character of Ni-Fe, W-Ni-Fe heavy alloys can be tested through a weight-specific saturation magnetization.
In this thesis, the saturation magnetization was measured with a permanent magnet (Koerzimat CS 1.096, Institut Dr. Foerster) with a nickel material constant. The mass and density of the sample had to be known. The sample was put in the magnet and after it got magnetized, it was pulled out steadily.

Die approbierte gedruckte Originalversion dieser Diplomarbeit ist an der TU Wien Bibliothek verfügbar
The approved original version of this thesis is available in print at TU Wien Bibliothek.
TU Bibliothek Your knowledge hub WIEN

3.3.4 Young's modulus

The Young's modulus (E) is a measure of the stiffness of a material. It is defined as the ratio of tensile stress (σ) to tensile strain (ϵ), see equation 2.

$$E = \frac{\sigma}{\epsilon} \tag{2}$$

The Young's modulus can be determined either with a static or dynamic method. For the dynamic method, a sample with a defined geometry was put on two taut wires. A metal tip then hit the sample and the resulting sound waves were recorded by a microphone and transferred to the detection system (RFDA Professional, IMCE). From the program, the Young's modulus could be directly calculated. The static Young's modulus was measured on the dumbbell-shaped tensile samples, see section 3.1.4. The Young's modulus can be also determined through the linear part of the stress-strain curves. The proportionality of stress to strain is given in Hookes' law with its coefficient, the Young's modulus.

3.3.5 Microscopy

To see the microstructure of the samples, a light optical microscope (Olympus GX51) was used. This was mainly used to get a quick overview of the self-produced binder materials. The pores were already visible with the light optical microscope.

For further and more precise investigations of the structure of the material, a scanning electron microscope (SEM) with SE (secondary electrons) and BSE (back scattered electrons) detectors was used. With the same device, EDX measurements were also performed on the samples. Within this thesis, the WHAs were investigated on the device QUANTA 200 from FEI.

3.3.6 XRD

To analyze the structures of compounds, X-ray diffraction (XRD) is used. This method gives information about crystal structures, phase compositions and the size of crystallites. The measured diffractograms are compared to reference patterns. The binder materials of this thesis were investigated on a Bragg-Brentano diffractometer PANalytical X'Pert Pro MPD in the X-Ray Center of TU Wien. The software for the used database is Highscore plus. For the measurements a semi conductor and CuK_α irradiation was used. 2θ varied from 20 to 130°.

Die approbierte gedruckte Originalversion dieser Diplomarbeit ist an der TU Wien Bibliothek verfügbar
The approved original version of this thesis is available in print at TU Wien Bibliothek.
TU Bibliothek Your knowledge hub WIEN

3.3.7 DTA

Differential thermal analysis (DTA) was used to determine the exact melting point of the binder materials. In this method, the temperature of the investigating sample and a reference material are exposed to the same heating program and in the process, the difference in temperature of both samples was measured. For DTA a small piece of only a few mm length of the binder material was used and put in argon atmosphere. The temperature program started at room temperature and went up to 1500 °C with a heating rate of 10 K/min. The device used in this thesis was STA 449 F3 Jupiter from Netzsch.

3.3.8 Low-temperature properites

The specific electrical resistivity and its reciprocal value, the electrical conductivity are in many cases much easier to determine than the thermal conductivity. To determine the thermal conductivity nevertheless, it can be derived via a simple ratio, [15]. This relationship between electrical and thermal conductivity in metals as a function of temperature is described by the Wiedemann-Franz law, equation 3.

$$L \cdot T = \frac{\lambda}{\sigma} \tag{3}$$

The thermal conductivity (λ) is directly proportional to the electrical conductivity (σ) and directly proportional to the temperature and the Lorenz number (L). The Lorenz number is directly proportional to the absolute temperature and should be constant for all metals, equation 4.

$$L_0 = \frac{\pi^2}{3} \cdot \frac{{k_B}^2}{e} = 2.44 \cdot 10^{-8} \frac{V^2}{K^2} \tag{4}$$

With the Boltzmann's constant (k_B) and the elementary charge (e). L_0 depends on the material and temperature. Both, electrical and thermal conductivity are a result of electron conduction.
In this work, the Wiedemann-Franz law is considered to infer from the electrical to the thermal conductivity. With different heat treatments, the electrical and thermal conductivity changes and the changes of thermal conductivity are according to the Wiedemann-Franz law proportional to, the electrical conductivity. The dependency of the electrical and thermal conductivity on the temperature can be observed by measuring the thermal or electrical conduction from 4 K to ambient. In [16], diamond composites were investigated, which showed an influence on the matrix composition.

Die approbierte gedruckte Originalversion dieser Diplomarbeit ist an der TU Wien Bibliothek verfügbar
The approved original version of this thesis is available in print at TU Wien Bibliothek.
TU Bibliothek Your knowledge hub WIEN

The residual resistivity ratio, RRR, is the ratio of the electrical conductivity at 273.15 K to the electrical resistivity at 4.2 K, equation 5 [17]. RRR is a measure of the quality of a sample. The higher this value, the purer the sample. The impurities relate not only to chemical impurities, but also to the shaping and processing that lead to defects within the material or on their surfaces [18], [19].

$$RRR = \frac{\rho(273.15K)}{\rho(4.2K)} \tag{5}$$

The low-temperature measurements were carried out at the Institute of Solid-State Physics at TU Wien. For this purpose, the samples had to be prepared in a specific way beforehand.

Binder materials according to the principle described in section 3.2.1 were produced. The samples were sintered at 1250 °C for 2 h in argon atmosphere. Those samples were then melted in a copperboat induction furnace under argon atmosphere at the Institute of Solid-State Physics at TU Wien.
To measure at low temperatures down to 4.2 K a four-point method is used [20]. The schematic setup is shown in figure 8a. This device only allows samples to be exactly 1 x 1 x 10 mm with all faces being plane-parallel. The samples were cut to this specific dimension with a semi-automatic precision cutting machine (Accutom-50, Struers). Due to the small dimensions of the sample, each sample was embedded for easier cutting. Four gold wires were welded to each of the samples and attached with a conductive adhesive (2-component silver), see figure 8b. This sample preparation is done on a PPMS (Physical Properties Measurements) - Puck, on which each sample and their four gold wires are fixed with an isolating adhesive "GE-Varnish", see figure 9a, 9b. This whole setup is then placed into the so-called "LuBer" - mount and cooled down to 4.2 K with a bath cryostat. The subsequent heating to room temperature is simply done by heating up the system itself. The measuring time of the individual resistors is only a few seconds [20].

Die approbierte gedruckte Originalversion dieser Diplomarbeit ist an der TU Wien Bibliothek verfügbar
The approved original version of this thesis is available in print at TU Wien Bibliothek.

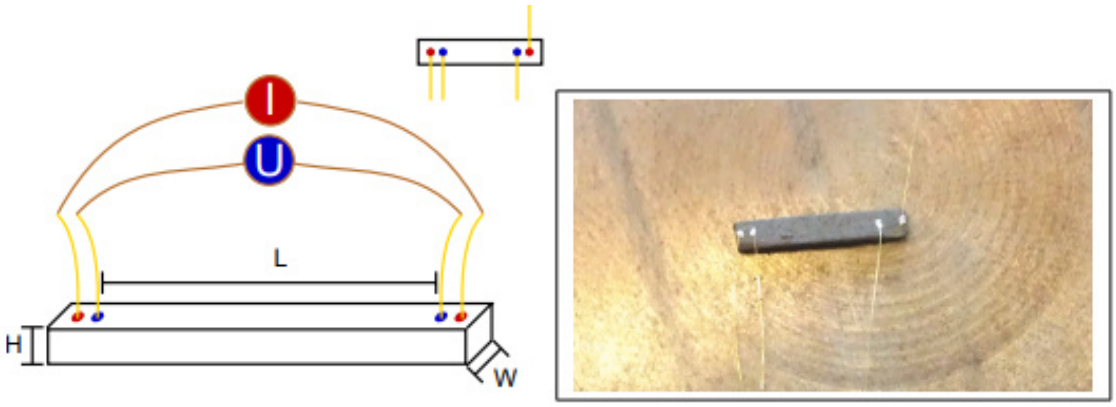

(a) **(b)**

Fig. 8: (a) Schematic measurement setup and (b) sample with gold wires [20].

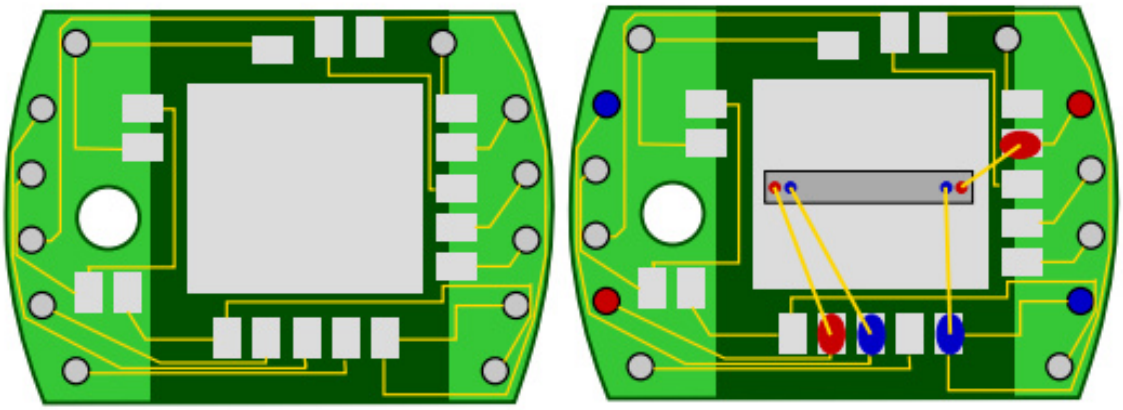

(a) **(b)**

Fig. 9: (a) Empty puck and (b) puck with the sample and their gold wires welded to the puck for a 4He system. On the blue marks, the voltage drop and on the red marks the current flow is measured [20].

Die approbierte gedruckte Originalversion dieser Diplomarbeit ist an der TU Wien Bibliothek verfügbar
The approved original version of this thesis is available in print at TU Wien Bibliothek.

4 Results and Discussion

4.1 Kinetics

4.1.1 Specific electrical resistivity

The samples were annealed in a furnace at different temperatures for different time periods. The annealing times were either 2 h, 20 h or 120 h. For all 4 different materials, the measurement of electrical resistivity was repeated 4 times on each heat treatment and annealing time to determine the measuring accuracy of the method itself. The reproducibility of the heat treatments was checked by comparing two batches of samples. The annealing temperature was varied between 800 and 1300 °C. Additionally, another batch with new samples was annealed exactly the same way. This second batch was only annealed at temperatures from 900 to 1300 °C for 2 h and at 1200 °C for 120 h.

The four following properties of each material were measured: specific electrical resistivity, thermal conductivity, saturation magnetization and Young's modulus, as described in section 3.3.

In figures 10a, 10b and 10c the specific electrical resistivity is plotted against the annealing temperature. The annealing time was exactly 2 h. In figure 10a the results of the first batch of the samples are depicted and in figure 10b the results of the second batch is plotted. In each of these figures, the mean value of the 4 measurements on one sample is depicted. If the deviation between those 4 measurements is significant, the standard deviation is visible as error bars. Figure 10c shows the comparison of both batches. In this figure, the error bars show the mean value of 8 measurements on each sample.

Die approbierte gedruckte Originalversion dieser Diplomarbeit ist an der TU Wien Bibliothek verfügbar
The approved original version of this thesis is available in print at TU Wien Bibliothek.

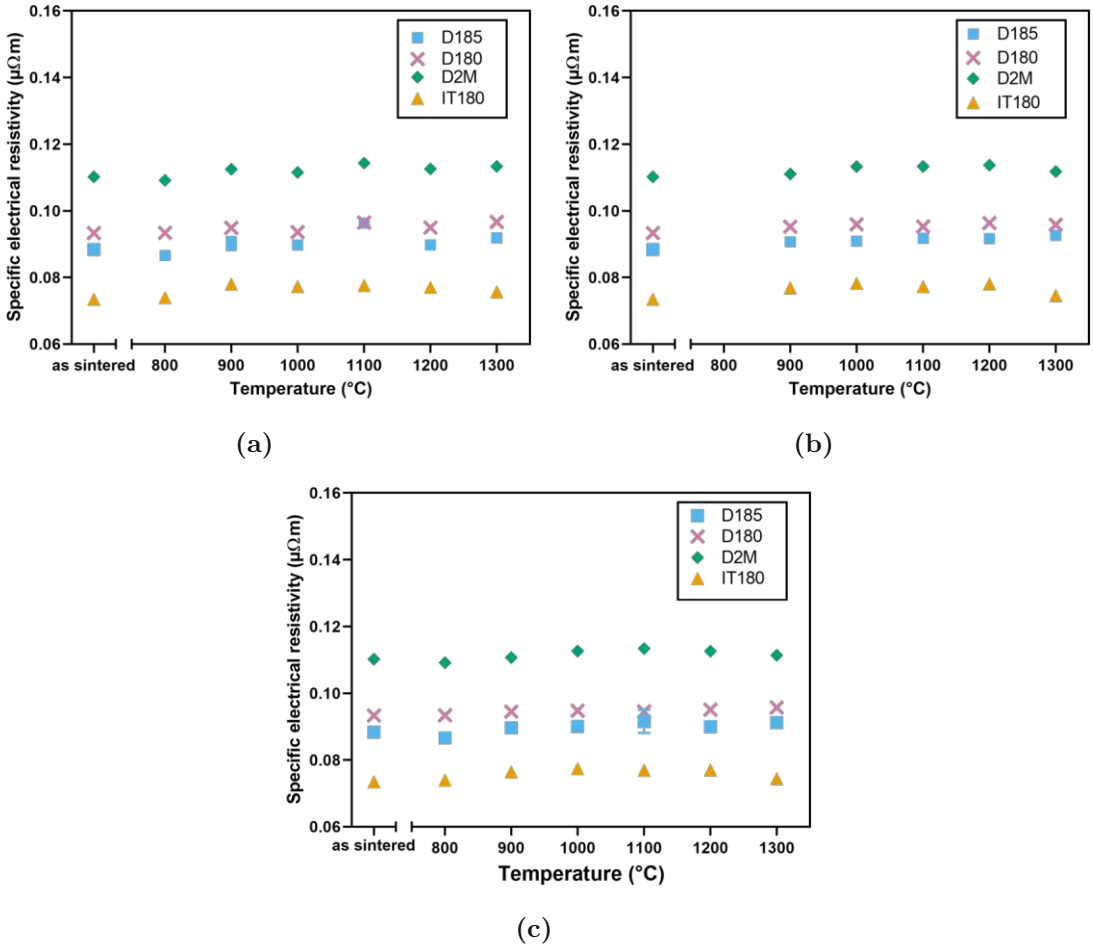

Fig. 10: Specific electrical resistivity measured in the as-sintered state and from 800 to 1300 °C for 2 hours - 1. batch (a), Specific electrical resistivity measured from 900 to 1300 °C for 2 hours - 2. batch (b), Comparison of 1. and 2. batch (c)

In figures 10a and 10b almost no significant changes between the measurements occur, due to the good reproducibility. Figure 10c shows, that the reproducibility is given not only for the measurements on one sample, but also, for two different samples, that were annealed and measured the exact same way. However, there is a conspicuous change between the two batches at the data point of 1100 °C of sample D185. The specific electrical resistivity varies from 0.096 $\mu\Omega$m of batch one to 0.091 $\mu\Omega$m of batch two.

In figures 11a, 11b and 11c the same procedure as described above was performed. The only difference is the annealing period. Before, the samples were annealed for 2 h. In the following figure, the annealing time was 120 h. Again, in

Die approbierte gedruckte Originalversion dieser Diplomarbeit ist an der TU Wien Bibliothek verfügbar
The approved original version of this thesis is available in print at TU Wien Bibliothek.
TU Bibliothek Your knowledge hub WIEN

figure 11a the first batch of the samples is shown and in figure 11b the second batch is demonstrated. The second batch only contains heat treatment at 1200 °C for 120 h. Figure 11c shows the mean value of the two batches.

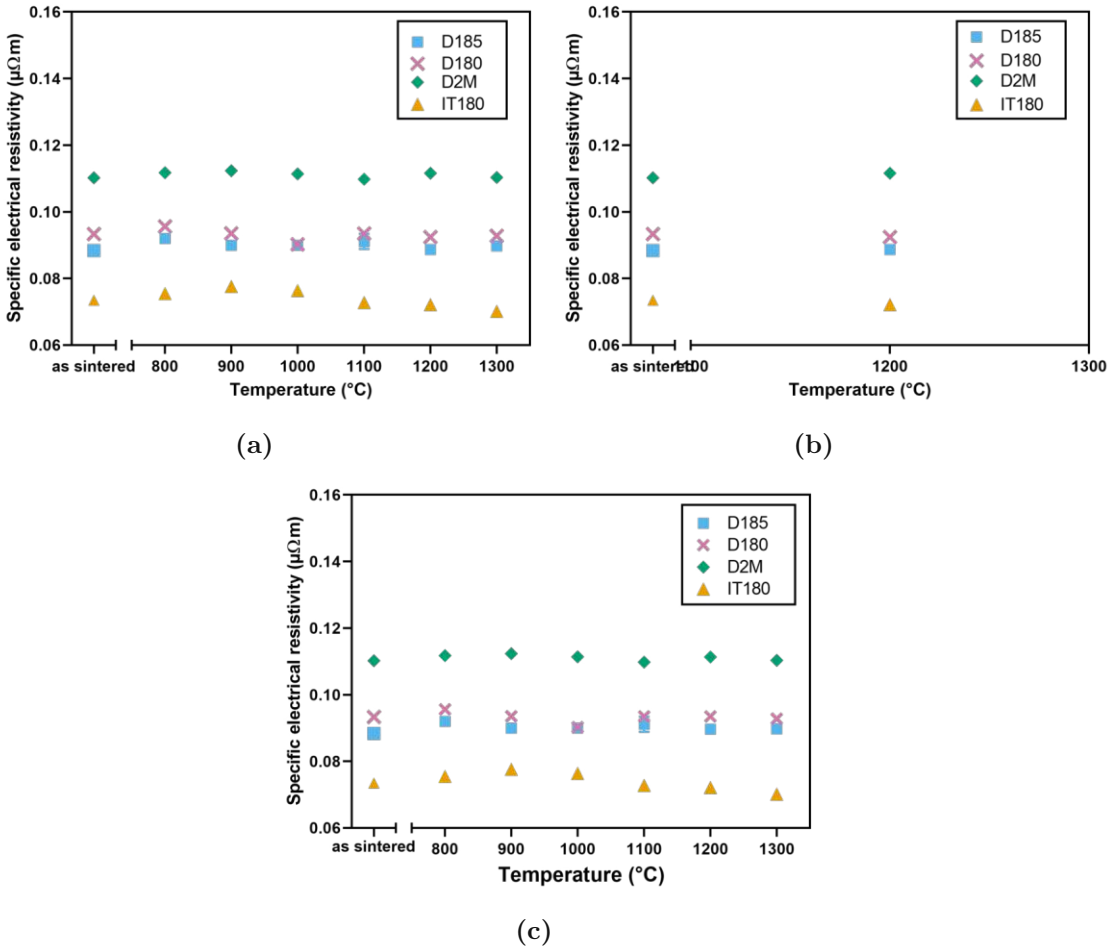

Fig. 11: Specific electrical resistivity measured in the as-sintered state and from 800 to 1300 °C for 120 hours - 1. batch (a), Specific electrical resistivity measured at 1200 °C for 120 hours - 2. batch (b), Comparison of 1. and 2. batch (c)

No significant changes between the 4 measurements of the specific electrical resistivity on each sample are visible, so a possible measuring inaccuracy can be excluded. At 1200 °C the values for each sample remain the same for two separate samples, annealed and measured the same way.

To detect the impact of the kinetics on the specific electrical resistivity, the two figures of the mean values of 2 h and of 120 h annealing time were compared in figure 12.

Die approbierte gedruckte Originalversion dieser Diplomarbeit ist an der TU Wien Bibliothek verfügbar
The approved original version of this thesis is available in print at TU Wien Bibliothek.
TU Bibliothek Your knowledge hub WIEN

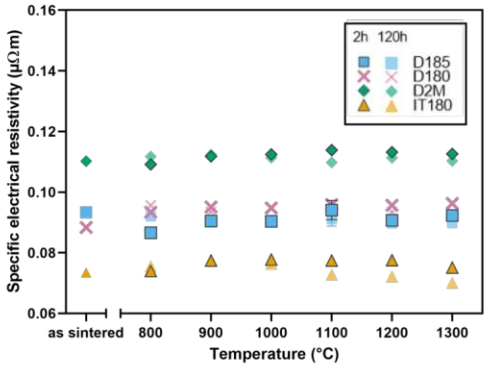

Fig. 12: Comparison of specific electrical resistivity measured for 2 hours (dark symbols) and 120 hours (pale symbols)

In general, the specific electrical resistivity of the samples annealed for 2 h is quite similar to the specific electrical resistivity of the samples annealed for 120 h. Some exceptions provide the materials D2M and IT180. The data point for D2M at 800 °C annealed for 120 h is slightly higher than the as-sintered sample and the sample annealed for 2 h. At 1100 °C, the data point of 120 h annealing time is lower than the one annealed for only 2 h. However, not much changed compared to the as-sintered state.
The material IT180 shows more dependence on kinetics. From 1100 °C on, the specific electrical resistivity of samples annealed for 120 h decrease compared to the electrical resistivity of the samples annealed for 2 h.

The changes in D2M and IT180 of specific electrical resistivity for longer annealing times most likely occur from diffusion processes. However, the change in D2M at 800 °C cannot really be explained by diffusion processes, since the temperature would be too low.

To see if the same effects, that appear at 120 h annealing time, occur at lower annealing times, heat treatments for 20 h were executed. Here, only a few temperatures were selected: 1000, 1100, and 1200 °C. In figure 13a the data of the 20 h annealing time was compared to the data of the 2 h annealing time. For the materials D185 and D180 there is no crucial difference between the two data sets recognizable. For D2M the data set for 20 h annealing time is lower than the one for 2 h. IT180 shows a lower value for 20 h in comparison to 2 h at 1200 °C. To decrease the specific electrical resistivity at 1200 °C, the material has to be annealed for more than 2 h.
The data of the 20 h annealed samples was compared to the data of the 120 h

Die approbierte gedruckte Originalversion dieser Diplomarbeit ist an der TU Wien Bibliothek verfügbar
The approved original version of this thesis is available in print at TU Wien Bibliothek.

annealed samples in figure 13b. D185, D180, and D2M do not show significant changes. However, IT180 shows a lower data point at 1100 °C for 120 h than for 20 h. At 1200 °C the values of IT180 for 20 h and for 120 h are the same. This means, that at this temperature, the material has the same specific electrical resistivity when annealed for a shorter time period.

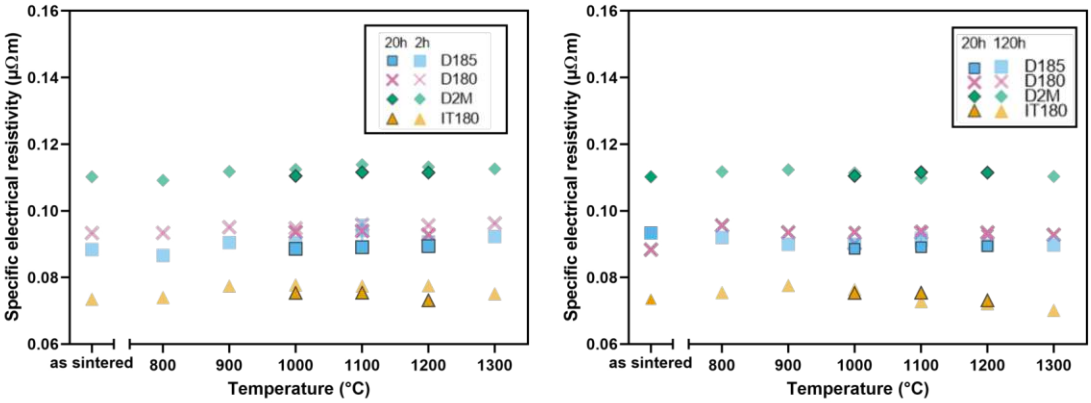

(a) **(b)**

Fig. 13: Comparison of the specific electrical resistivity measured for 20 h (dark symbols) and for 2 h (pale symbols) (a), Comparison of the specific electrical resistivity measured for 20 h (dark symbols) and for 120 h (pale symbols) (b)

As stated in [7], consecutive heat treatments provide different results. In this work, the materials seem to have a memory, since the values change with each heat treatment. For the specific electrical resistivity, respectively, the values for D185, D180, D2M and IT180 rise with higher annealing temperatures and are higher than the as-sintered values. A phenomenon that cannot be observed in this thesis, where each sample experiences only one heat treatment.
Therefore, further experiments, namely consecutive heat treatments, were carried out with the four materials. Two different consecutive heat treatments were executed, section 3.1.3.
In the first experiment, one sample of each material was annealed at 1200 °C for 120 hours and then measured. Afterward, each of those samples was annealed again. This time at 1000 °C for two hours. The data for the specific electrical resistivity for the described experiment is found in figure 14a.
In the second experiment, one sample of each material was annealed at 1300 °C for 120 hours and then measured. Then, each of those samples was annealed again at 800 °C for two hours. After letting the samples cool down and measuring the properties again, the samples were heated up to 1000 °C once more and after

Die approbierte gedruckte Originalversion dieser Diplomarbeit ist an der TU Wien Bibliothek verfügbar
The approved original version of this thesis is available in print at TU Wien Bibliothek.
TU Bibliothek Your knowledge hub WIEN

cooling down measured to get the properties of each material.

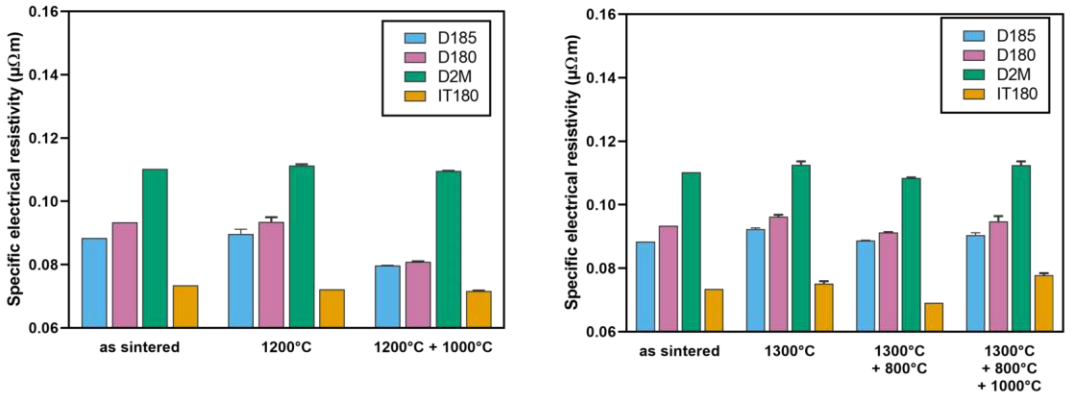

(a) **(b)**

Fig. 14: Specific electrical resistivity after consecutive heat treatment at 1200 °C for 120 h - new as-sintered state - at 1200 h for 2 h and 1000 °C for 2 h (a), 1300 °C for 120 h - new as-sintered state - at 1300 2h, 800 °C for 2 h and 1000 °C for 2 h (b)

Figure 14a exposes, that the specific electrical resistivity for D185 and D180 decrease with another annealing treatment.

Figure 14b indicates that all values decrease slightly when annealed at 1300 °C first and then annealed at 800 °C. On the contrary, they increase again when additional annealing of 1000 °C was conducted.

Compared to [7], the values of all materials are at any heat treatment significantly lower, even in the initial state. Whereas in [7], the values increased slightly, there is now no longer any trend to be seen.

The electrical resistivity in the product data sheets is between 0.1 and 0.17 $\mu\Omega$m. The values of the specific electrical resistivity, measured after all different heat treatments described above, are significantly below these values. This might be due to different equipments and different operators.

4.1.2 Thermal conductivity

In this section the exact same approaches were done as described in 4.1.1, however, the influence of different annealing parameters was observed on thermal conductivity instead of specific electrical resistivity.

Die approbierte gedruckte Originalversion dieser Diplomarbeit ist an der TU Wien Bibliothek verfügbar
The approved original version of this thesis is available in print at TU Wien Bibliothek.
TU Bibliothek Your knowledge hub WIEN

Due to initial difficulties in measuring thermal conductivity, a pure tungsten rod was added to the heat treatment as a comparison sample. The tungsten rod, as expected, did not change its properties after several heat treatments of only up to 1300 °C. The measured thermal conductivity was 172 W/m*K. The thermal conductivity found in literature is 175 W/m*K at room temperature, [21].

Figure 15a shows the measured thermal conductivity of the first batch of samples annealed at temperatures from 800 to 1300 °C for 2 h annealing time. In this figure, error bars are visible for 900 and 1300 °C. Figure 15b displays the second batch of samples annealed only at temperatures from 1000 to 1300 °C.

In figure 15c the values of both batches above are compared. Here, the error bars show the deviation of the two batches.
The data of all materials annealed for 2 h have a small peak at 900 °C. While the data of D185, D180 and D2M annealed for 2 h remain mainly constant, the one for IT180 rises with higher temperature. However, at 1300 °C the thermal conductivity for IT180 is only at 94.6 W/m*K compared to 97.3 W/m*K at 900 °C.

Die approbierte gedruckte Originalversion dieser Diplomarbeit ist an der TU Wien Bibliothek verfügbar
The approved original version of this thesis is available in print at TU Wien Bibliothek.
TU Bibliothek Your knowledge hub WIEN

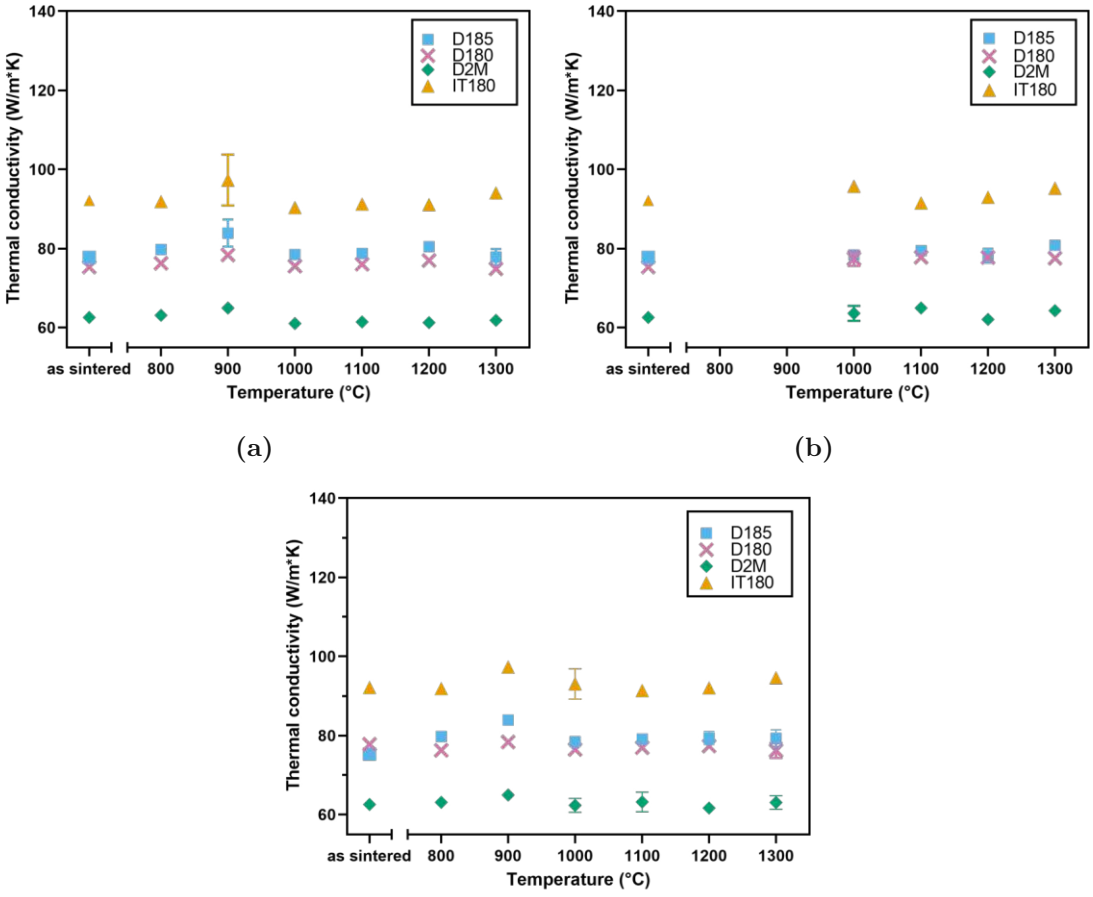

Fig. 15: Thermal conductivity measured in the as-sintered state and from 800 to 1300 °C for 2 hours - 1. batch (a), thermal conductivity measured from 900 to 1300 °C for 2 hours - 2. batch (b), Comparison of 1. and 2. batch (c)

In the following, the thermal conductivity is plotted against the temperature for the samples annealed for 120 h. Figure 16a presents the first batch of the samples and figure 16b shows the second batch, only annealed at 1200 °C. The combination of both batches with standard deviation is displayed in figure 16c.

Die approbierte gedruckte Originalversion dieser Diplomarbeit ist an der TU Wien Bibliothek verfügbar
The approved original version of this thesis is available in print at TU Wien Bibliothek.

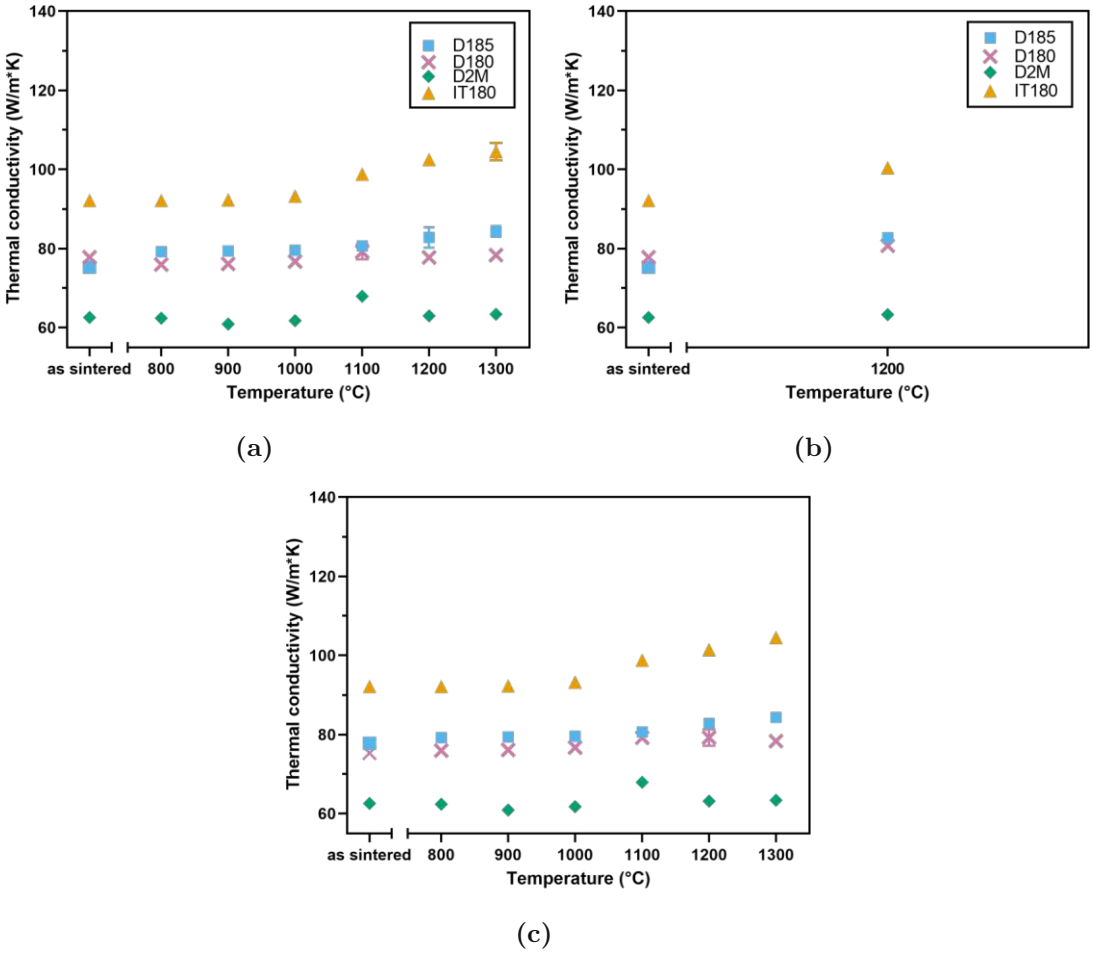

Fig. 16: Thermal conductivity measured in the as-sintered state and from 800 to 1300 °C for 120 hours - 1. batch (a), thermal conductivity measured at 1200 °C for 120 hours - 2. batch (b), Comparison of 1. and 2. batch (c)

When looking at the data of the samples that were annealed for 120 h, the maxima at 900 °C disappeared. D2M now has a maxima at 1100 °C. The data set of D180 remains mainly constant. The thermal conductivity of D185 and IT180 rises with higher temperatures.

In figure 17 the thermal conductivity of the samples annealed for 2 h is compared to the ones annealed for 120 h. Here, the influence of the annealing time on the change in temperature is more clearly visible from an annealing temperature of 1000 °C.

Die approbierte gedruckte Originalversion dieser Diplomarbeit ist an der TU Wien Bibliothek verfügbar
The approved original version of this thesis is available in print at TU Wien Bibliothek.

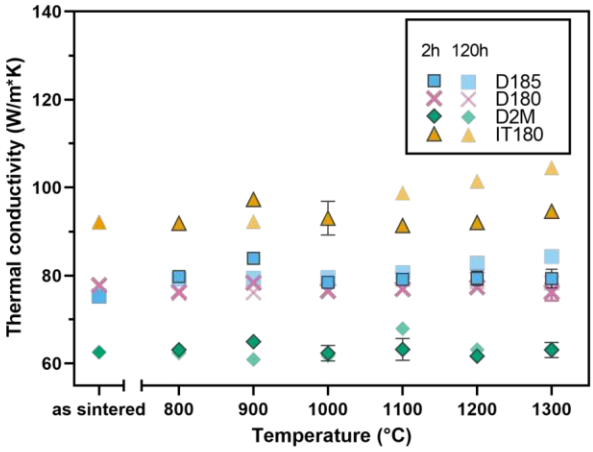

Fig. 17: Comparison of thermal conductivity measured for 2 hours (dark symbols) and 120 hours (pale symbols)

The rise in thermal conductivity with temperature in both annealing times could be due the enhancement of the conductivity of interfaces [22], [23].

As described in section 4.1.1 the samples were also annealed for 20 h at 1000, 1100 and 1200 °C.

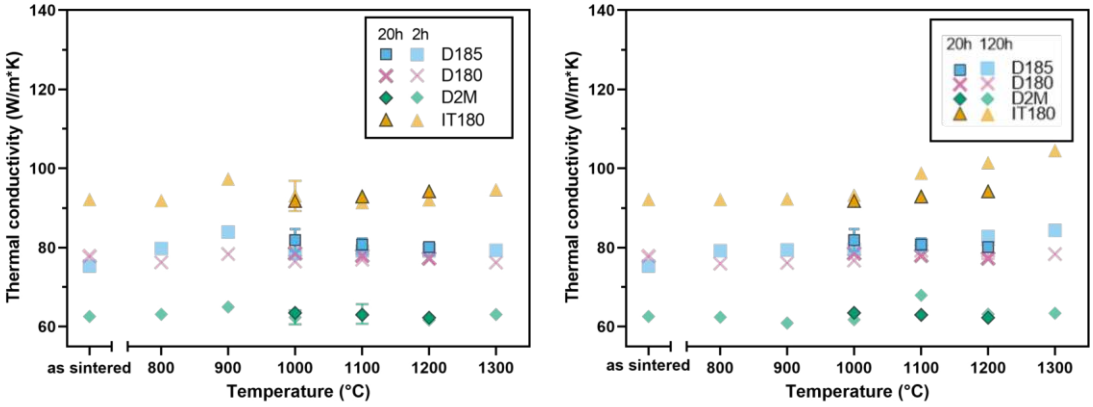

(a) **(b)**

Fig. 18: Comparison of the thermal conductivity measured for 20 h (dark symbols) and for 2 h (pale symbols) (a), Comparison of the thermal conductivity measured for 20 h (dark symbols) and for 120 h (pale symbols) (b)

The data set of the samples that were annealed for 20 h is almost congruent to the data set of 2 h , see figure 18a.
When compared to the thermal conductivity of 120 h, the difference in the material

Die approbierte gedruckte Originalversion dieser Diplomarbeit ist an der TU Wien Bibliothek verfügbar
The approved original version of this thesis is available in print at TU Wien Bibliothek.

IT180 is better visible. It seems that 20 h are not sufficient to the high rise of the thermal conductivity from 1000 °C on.

Two experiments of consecutive heat treatments, as already described in section 4.1.1, were executed. In the first experiment the samples were measured at 1200 °C and subsequently at 1000 °C for 2 h each. In the second experiment the samples were firstly annealed at 1300 °C, then at 800 °C and finally at 1000 °C. This is discussed below and shown in figures 19a and 19b.
Figure 19a shows that the thermal conductivity of all materials rises with consecutive heat treatment.
In the second experiment, figure 19b, the same results apply as in the consecutive heat treatment experiment described above. The thermal conductivity of all materials rises with consecutive heat treatment. In comparison, the thermal conductivity in [7], decreases with consecutive heat treatment. In contrast to the specific electrical resistivity, the values in both works are in the same range. In [24], material D185 was also measured. The results are similar to this thesis, namely, the values of thermal conductivity are at around 80 - 90 W/m*K and thermal conductivity increases with higher temperature.

The values measured in this work agree well with the data sheets, [1], being in the range of 70 - 110 W/m*K for samples D185, D180 and IT180.

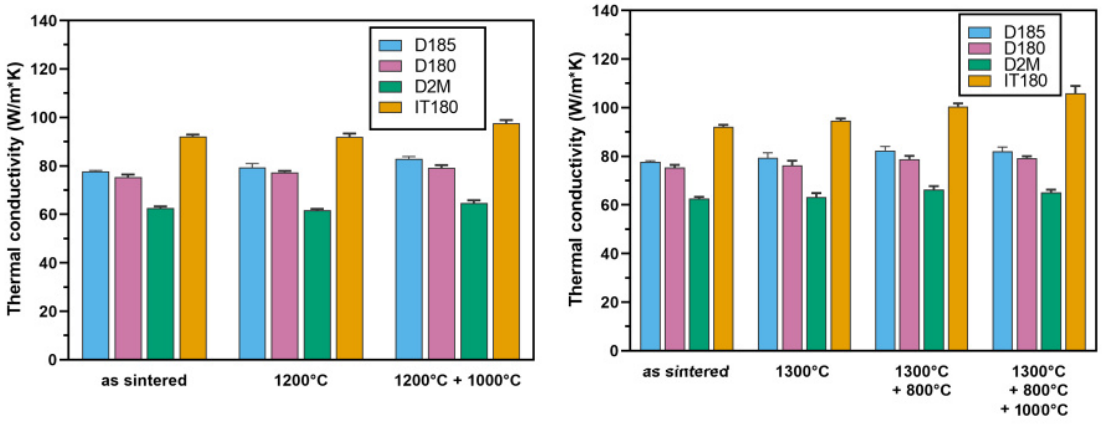

(a) **(b)**

Fig. 19: Thermal conductivity after consecutive heat treatment at 1200 °C for 120 h - new as-sintered state - at 1200 h for 2 h and 1000 °C for 2 h (a), 1300 °C for 120 h - new as-sintered state - at 1300 2h, 800 °C for 2 h and 1000 °C for 2 h (b)

Die approbierte gedruckte Originalversion dieser Diplomarbeit ist an der TU Wien Bibliothek verfügbar
The approved original version of this thesis is available in print at TU Wien Bibliothek.

4.1.3 Saturation magnetization

In the following, the results of the measurements of the saturation magnetization are depicted. Repeatedly, the two batches of samples measured for 2 h are shown in figure 20a and figure 20b. The standard deviation of the 4 measurements on each sample is considered in figures 20a and 20b. The mean value of those two batches is plotted in figure 20c.

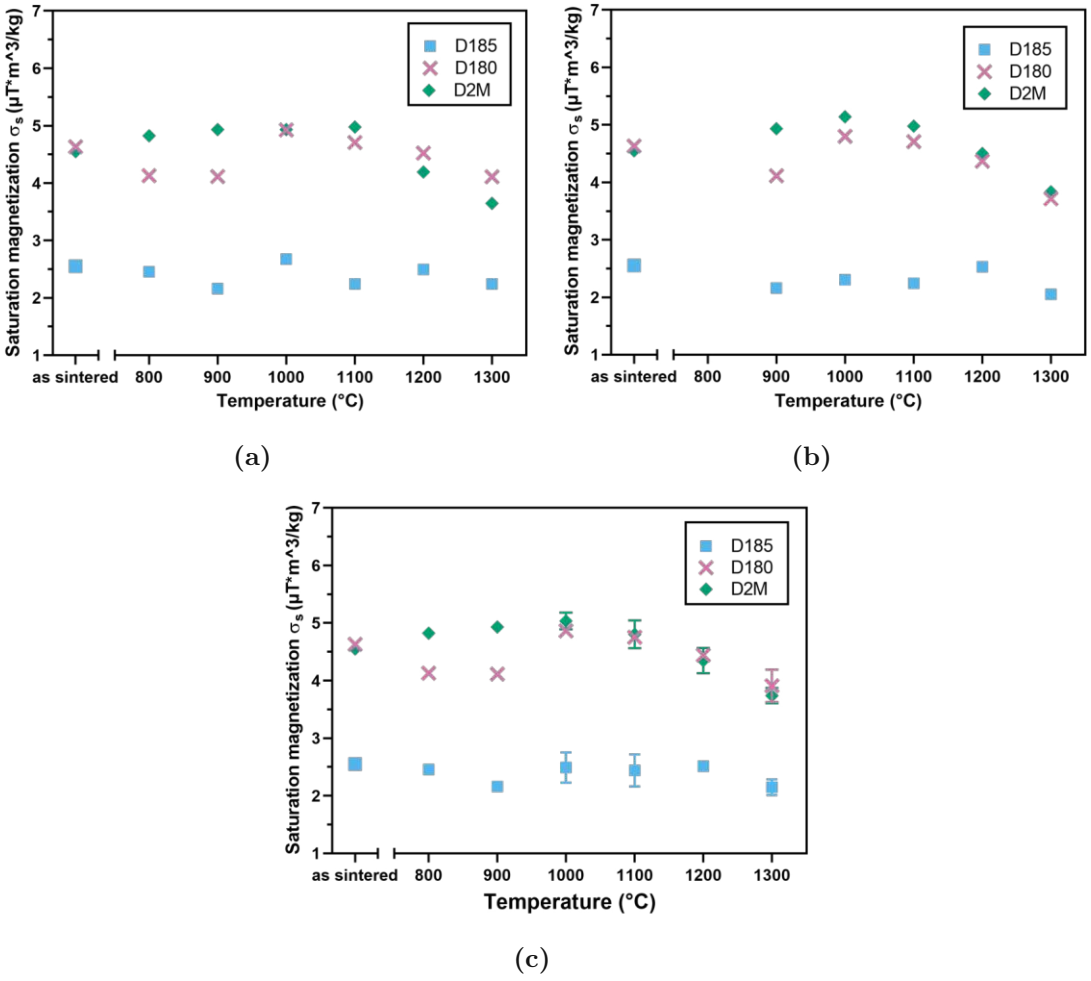

Fig. 20: Saturation magnetization measured in the as-sintered state and from 800 to 1300 °C for 2 hours - 1. batch (a), saturation magnetization measured from 900 to 1300 °C for 2 hours - 2. batch (b), Comparison of 1. and 2. batch (c)

The figures above show, that the reproducibility of the saturation magnetization is given. With higher temperatures, the saturation magnetization of all samples decreases. This trend fits the saturation magnetization of materials D185, D180 and D2M in [7].

Die approbierte gedruckte Originalversion dieser Diplomarbeit ist an der TU Wien Bibliothek verfügbar
The approved original version of this thesis is available in print at TU Wien Bibliothek.
TU Bibliothek Your knowledge hub WIEN

Interesting in figure 21c is the comparison of material D180 and D2M. While the as-sintered batches of both materials are quite similar, there is suddenly a larger gap between D180, that decreases, and D2M, that slightly increases, at temperatures of 800 and 900 °C. At 1100 °C the values of both materials are exactly the same and from there on, the saturation magnetization of both materials decrease.

In figures 21a and 21b the two batches of the samples annealed for 120 h are presented as described in the sections before. In figure 21c both batches are compared and plotted with their standard deviation.
As the saturation magnetization of the samples that were annealed for 2 h already shows, the saturation magnetization of 120 h annealing time also decreases with increasing temperature.
Interesting are the data points of the saturation magnetization at 800 and 900 °C. The saturation magnetization of D180 is at 800 °C lower than in the as-sintered state. From 800 to 900 °C the saturation magnetization increases drastically. D185 shows a similar trend. On the contrary, the saturation magnetization of D2M is higher at 800 °C than in the as-sintered state. At 900 °C the saturation magnetization reaches its minimum, that is just slightly lower than in the as-sintered state. At 1000 °C the saturation magnetization rises again and has now almost the same value as at 800 °C. From 900 °C on, the values of the saturation magnetization of both materials decrease again.

Die approbierte gedruckte Originalversion dieser Diplomarbeit ist an der TU Wien Bibliothek verfügbar
The approved original version of this thesis is available in print at TU Wien Bibliothek.

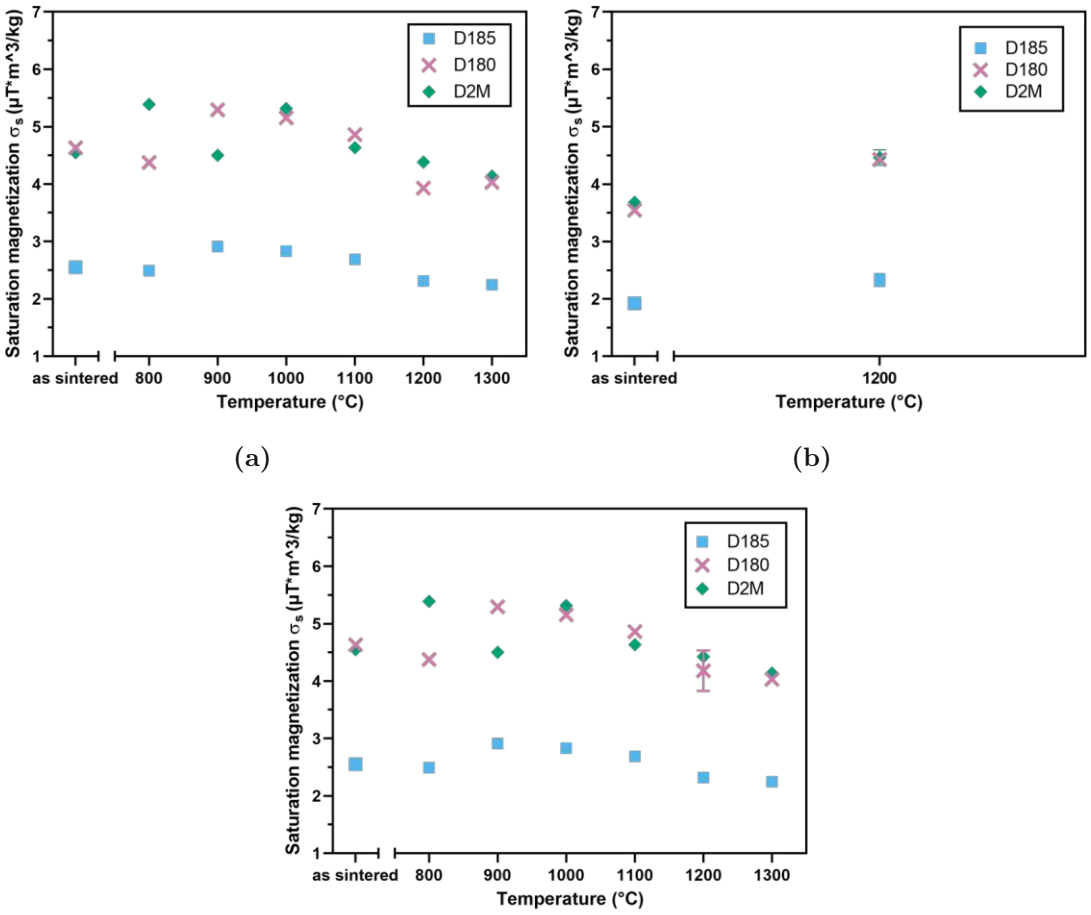

Fig. 21: Saturation magnetization measured in the as-sintered state and from 800 to 1300 °C for 120 hours - 1. batch (a), saturation magnetization measured from 900 to 1300 °C for 120 hours - 2. batch (b), Comparison of 1. and 2. batch (c)

The comparison between 2 h and 120 h annealing time shows the impact of the kinetic especially at lower temperatures, see figure 22. What is striking here is the change of the saturation magnetization of all materials at 900 °C. The saturation magnetization of D185 and D180 increases with longer annealing times. In contrast to that, the saturation magnetization of D2M decreases with longer annealing times. The values from 900 °C on also vary depending on the kinetics.

Die approbierte gedruckte Originalversion dieser Diplomarbeit ist an der TU Wien Bibliothek verfügbar
The approved original version of this thesis is available in print at TU Wien Bibliothek.

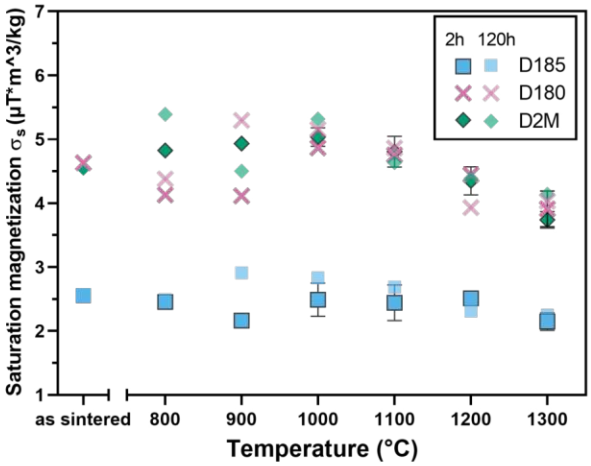

Fig. 22: Comparison of saturation magnetization measured for 2 hours (dark symbols) and 120 hours (pale symbols)

Since the annealing for 20 h was only performed between 1000 and 1200 °C, the differences are not that decisive. As mentioned before, the saturation magnetization of all materials shows the same trend from 1000 °C on. The decrease of the saturation magnetization is also seen in [3]. The binder is ferromagnetic. As more tungsten dissolves in the binder, the saturation magnetization must decrease. This theory is confirmed in figure 22, as the saturation magnetization decreases above 1100 °C.

D185 shows, with a value of 2.8 µT*m^3/kg, higher saturation magnetization at 1000 °C when annealed for 20 h in comparison to 2 h annealing time, see figure 23a. D180 shows, with a value of about 4.3 µT*m^3/kg, lower saturation magnetization at 1100 °C when annealed for 20 h in comparison to 2 h. D2M has congruent values, around 5.0 µT*m^3/kg, for both annealing times.
Compared to 120 h, the saturation magnetization of sample D185 annealed for 20 h, is, with a value of 2.4 µT*m^3/kg, lower at 1100 °C. For D180 the saturation magnetization is also lower at 1000 °C and 1100 °C. However, it is higher at 1200 °C, 4.5 µT*m^3/kg. For D2M the saturation magnetization is slightly lower for 20 h at 1000 °C, but higher at 1100 °C. At 1200 °C both values are congruent.

Die approbierte gedruckte Originalversion dieser Diplomarbeit ist an der TU Wien Bibliothek verfügbar
The approved original version of this thesis is available in print at TU Wien Bibliothek.
TU Bibliothek Your knowledge hub WIEN

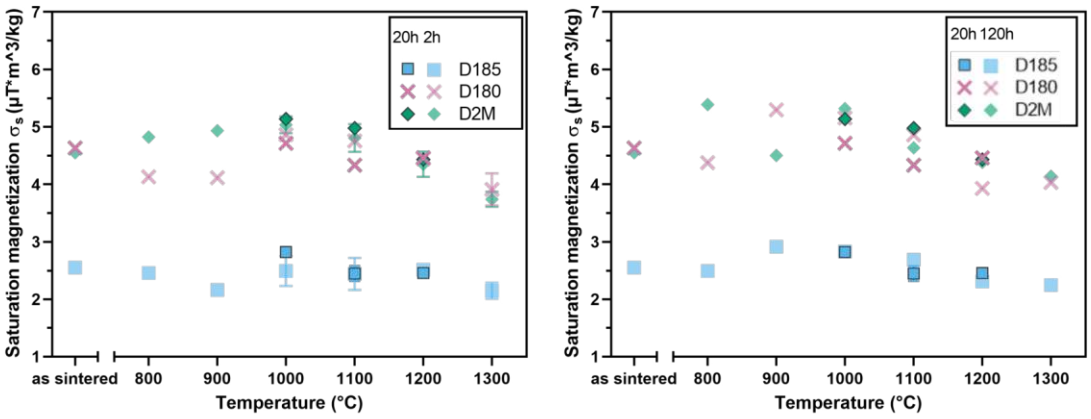

(a) **(b)**

Fig. 23: Comparison of the saturation magnetization measured for 20 h (dark symbols) and for 2 h (pale symbols) (a), Comparison of the saturation magnetization measured for 20 h (dark symbols) and for 120 h (pale symbols) (b)

The fact, that the saturation magnetization has lower values after heat treatment at higher temperatures, is also seen in the experiments with consecutive heat treatments.

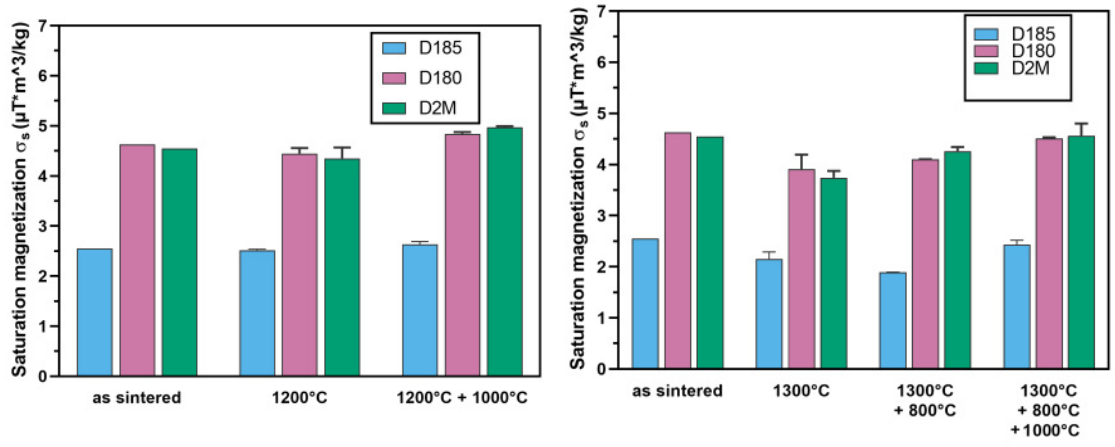

(a) **(b)**

Fig. 24: Saturation magnetization after consecutive heat treatment at 1200 °C for 120 h - new as-sintered state - at 1200 h for 2 h and 1000 °C for 2 h (a), 1300 °C for 120 h - new as-sintered state - at 1300 2h, 800 °C for 2 h and 1000 °C for 2 h (b)

In figure 24a the difference of the saturation magnetization between as-sintered and 1200 °C annealing temperature is more evident. The values of D180 and

Die approbierte gedruckte Originalversion dieser Diplomarbeit ist an der TU Wien Bibliothek verfügbar
The approved original version of this thesis is available in print at TU Wien Bibliothek.

D2M decrease slightly when the samples are annealed at 1200 °C. However, the standard deviations are within the range of the as-sintered values. The saturation magnetization of all materials increases when samples are firstly annealed at 1200 °C for 120 h and then again annealed at 1000 °C for 2 h.
The same trend is observable in the second experiment of consecutive heat treatments. Here, the gap between as-sintered and the first heat treatment is well visible. Then, with every further heat treatment at 800 °C and 1000 °C the saturation magnetization increases again. After the last heat treatment, the values are almost equal to the as-sintered values.

4.1.4 Young's Modulus

The Young's modulus of all samples annealed for 2 h stays quite constant with rising temperature, see figure 25a, 25b and 25c. Almost every material reaches its maximum at another temperature. While D185 is relatively steady and has its maximum already at 800 °C, D180 is the only material that has a lower value at 800 °C compared to the as-sintered state. The Young's modulus of D180 then rises and reaches its maximum at 1200 °C. At 1300 °C it reaches the value of the as-sintered state in the first batch. However, the second batch shows, that Young's modulus of D180 at 1200 °C equals the one at as-sintered and has its maximum at 1300 °C. The standard deviation between the two batches of D180 at 1300 °C is, with a value of 4.4, pretty high. D2M rises with higher temperature and then decreases again and finally has its maximum at 1300 °C. The maximum is already reached at 1000 °C in the first batch. However, all these changes in temperature are quite small and not significant.
The material IT180 shows an exception in the Young's modulus. In both batches, IT180 shows a significant increase of Young's modulus from 1200 °C to 1300 °C.

Die approbierte gedruckte Originalversion dieser Diplomarbeit ist an der TU Wien Bibliothek verfügbar
The approved original version of this thesis is available in print at TU Wien Bibliothek.
TU Bibliothek Your knowledge hub WIEN

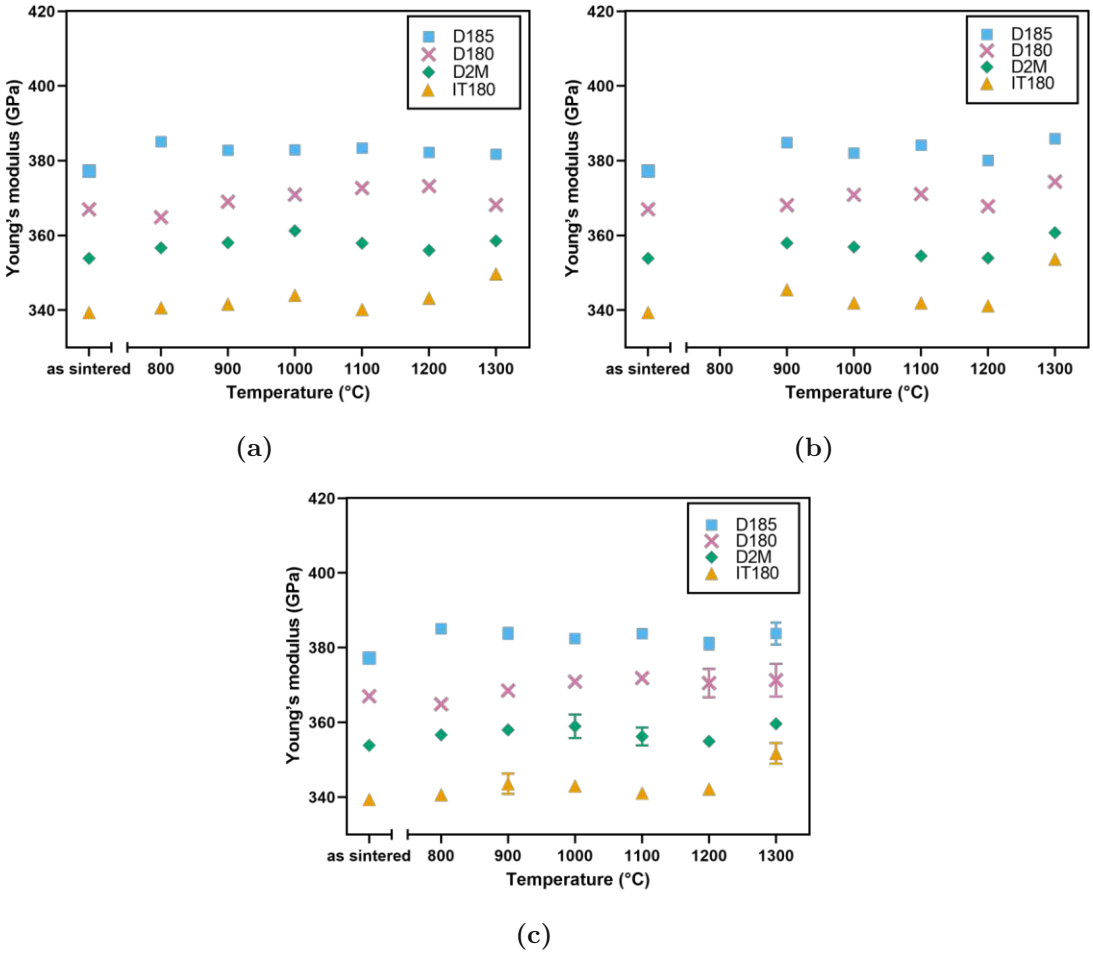

Fig. 25: Young's modulus measured in the as-sintered state and from 800 to 1300 °C for 2 hours - 1. batch (a), Young's modulus measured from 900 to 1300 °C for 2 hours - 2. batch (b), Comparison of 1. and 2. batch (c)

Batches one and two of samples annealed at 120 h, show the same trend, see figure 26a, 26b and 26c. An exception shows the Young's modulus at 1200 °C. The Young's modulus at this temperature varies in both batches.
Striking are again the values of IT180. This time the Young's modulus increases from 339 GPa, as-sintered, to 354 GPa at 1100 °C and then keeps rising up to 360 GPa at 1300 °C.

Die approbierte gedruckte Originalversion dieser Diplomarbeit ist an der TU Wien Bibliothek verfügbar
The approved original version of this thesis is available in print at TU Wien Bibliothek.

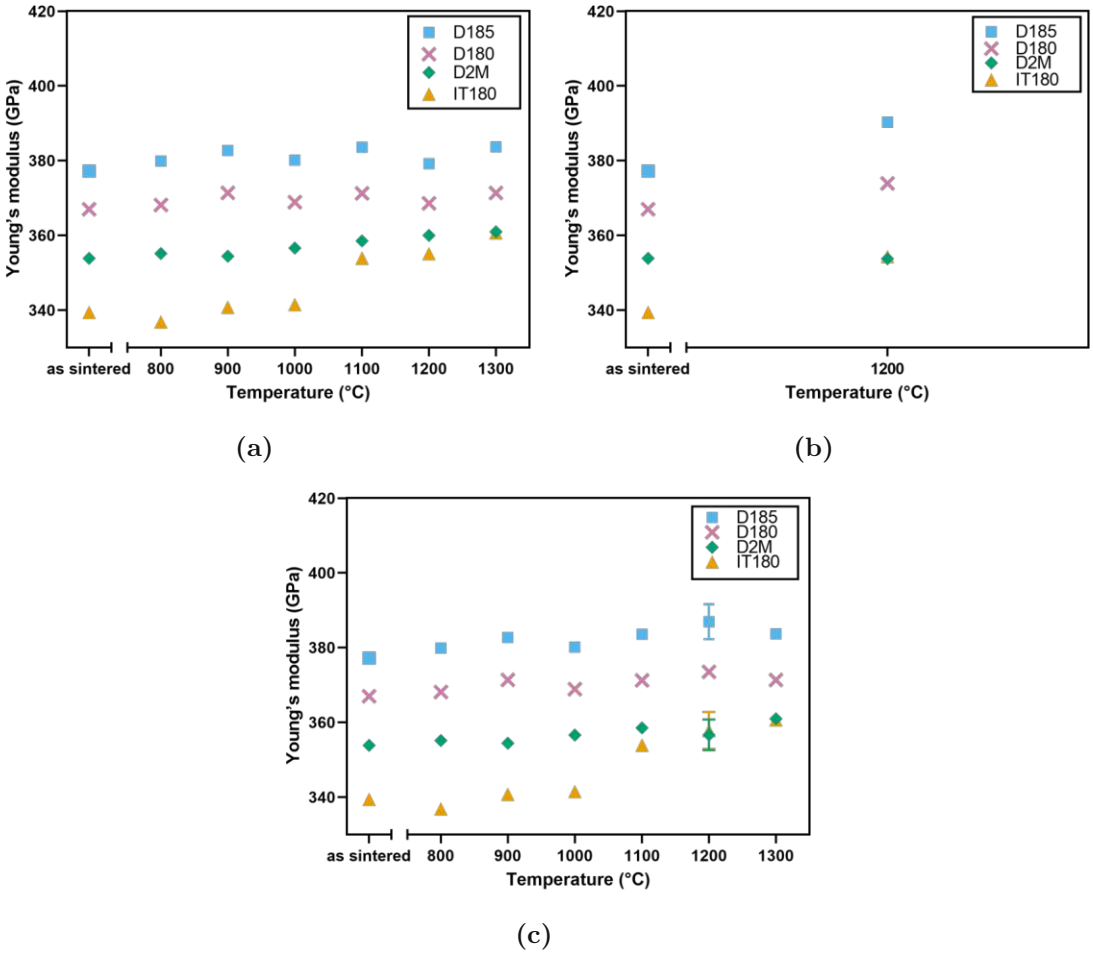

Fig. 26: Young's modulus measured in the as-sintered state and from 800 to 1300 °C for 120 hours - 1. batch (a), Young's modulus measured at 1200 °C for 120 hours - 2. batch (b), Comparison of 1. and 2. batch (c)

When the values of the 2 h annealing time are compared to the ones at 120 h in figure 27, the difference of IT180 is better visible.
With a shorter annealing time, Young's modulus of this material increases at 1300 °C. With a longer annealing period, Young's modulus increases at a lower temperature, 1100 °C.

Die approbierte gedruckte Originalversion dieser Diplomarbeit ist an der TU Wien Bibliothek verfügbar
The approved original version of this thesis is available in print at TU Wien Bibliothek.

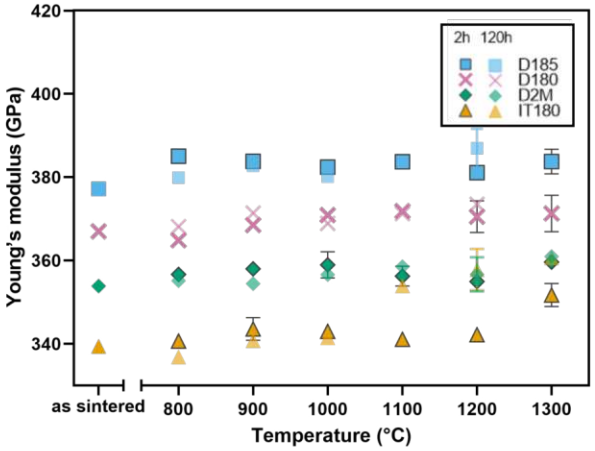

Fig. 27: Comparison of Young's modulus measured for 2 hours (dark symbols) and 120 hours (pale symbols)

The effects of the Young's modulus during the 20 h anneals can be seen in figure 28a and 28b.
Compared to 2 h annealing time, the values of D185, D180 and D2M of 20 h remain the same at temperatures 1000 and 1100 °C, see figure 28a. At 1200 °C a difference in all materials is visible between the two annealing periods. The value of D185 and D2M at 20 h is higher than the ones at 2 h annealing time. The value of D180 is lower at 20 h compared to 2 h annealing period.
The material IT180 shows more difference in annealing times than the other materials. Starting at 1000 °C there is yet not much difference between the annealing periods of 2 h and 20 h. However, the changes from 1100 °C and on are crucial. At 1100 °C the value increases from 341 GPa (2 h) to 346 GPa. At 1200 °C the Young's modulus increases to 354 GPa and therefore has a difference of 12 GPa to IT180 annealed for 2 h at 1200 °C.

As stated in the data sheets, [1], the Young's modulus for the materials D185, D180 and IT180 should be between 360 and 385 GPa. This fits the material D185. Material D180 is with values of about 370 GPa already lower than the value of 380 GPa stated in literature, [1]. IT180, however, is with its in this thesis measured values even 20 GPa lower than the 360 GPa given in literature and is therefore a major exception. With an annealing time of 2 h, IT180 at 1300 °C approaches the value of 360 GPa given in the literature. With an annealing time of 120 h, IT180 reaches the value already at 1200 °C.

In figure 28b, the values of 20 h annealing time are compared to the ones of

Die approbierte gedruckte Originalversion dieser Diplomarbeit ist an der TU Wien Bibliothek verfügbar
The approved original version of this thesis is available in print at TU Wien Bibliothek.
TU Bibliothek Your knowledge hub WIEN

120 h annealing time. D185 and D180 show a very similar trend. Firstly, at 1000 °C the Young's modulus of 20 h is higher than the one of 120 h annealing time. Then, at 1100 °C the values of both times are almost congruent. Lastly, at 1200 °C the values of 20 h are lower than at 120 h annealing time. D2M also shows higher values for 20 h annealing time compared to 120 h. However, there is not much difference at 1100 °C and 1200 °C.
The Young's modulus of IT180 also increases at 1000 °C. However, at 1100 °C the Young's modulus of 20 h is already lower than the one of 120 h. At 1200 °C the value of 20 h is still lower than the one of 120 h but due to the increase of the Young's modulus at this temperature, the difference now is only 4 GPa.
The Young's modulus of IT180 increases with higher temperature. With longer annealing times, the Young's modulus of this material starts to increase at lower temperatures.

Compared to literature, [1], the Young's modulus of IT180 approaches the 360 GPa at 1200 °C and 20 h annealing time. With an annealing time of 120 h the measured Young's modulus is still closer to the desired 360 GPa.

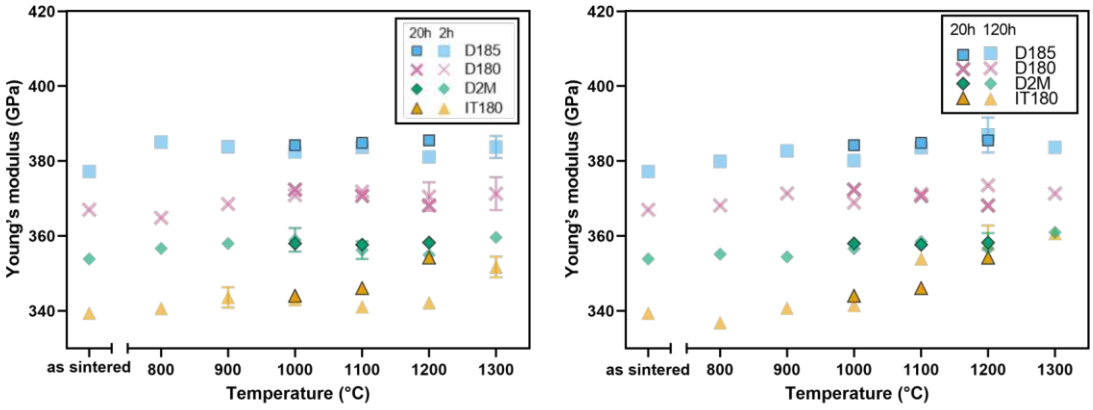

(a) **(b)**

Fig. 28: Comparison of Young's modulus measured for 20 h (dark symbols) and for 2 h (pale symbols) (a), Comparison of Young's modulus measured for 20 h (dark symbols) and for 120 h (pale symbols) (b)

To determine a clearer trend of Young's modulus, the experiments with gradual heat treatments should be considered. In the first experiment, the Young's modulus of each material increases with consecutive heat treatment, see figure 29a.
In the second experiment, Young's modulus increases from the as-sintered state when firstly annealed at 1300 °C for 120 h and then annealed at 800 °C for 2 h.

Die approbierte gedruckte Originalversion dieser Diplomarbeit ist an der TU Wien Bibliothek verfügbar
The approved original version of this thesis is available in print at TU Wien Bibliothek.
TU Bibliothek Your knowledge hub WIEN

When each material is then annealed again at 1000 °C the Young's modulus decreases again. So a peak after the second heat treatment is observable. From all materials, this trend is best visible for IT180.

With consecutive heat treatments, material IT180 reaches the 360 GPa given in literature, [1]. It even reaches its maximum value of about 370 °C when annealed at 1300 °C for 2 h and then at 800 °C for another 2 h. The reason why IT180 reaches the value of 360 GPa with consecutive heat treatments is, that an as-sintered condition is assumed here, in which the sample has already been annealed at 1200 °C for 120 h beforehand. As discussed above, this is the temperature and time, where IT180 reaches the Young's modulus of 360 GPa.

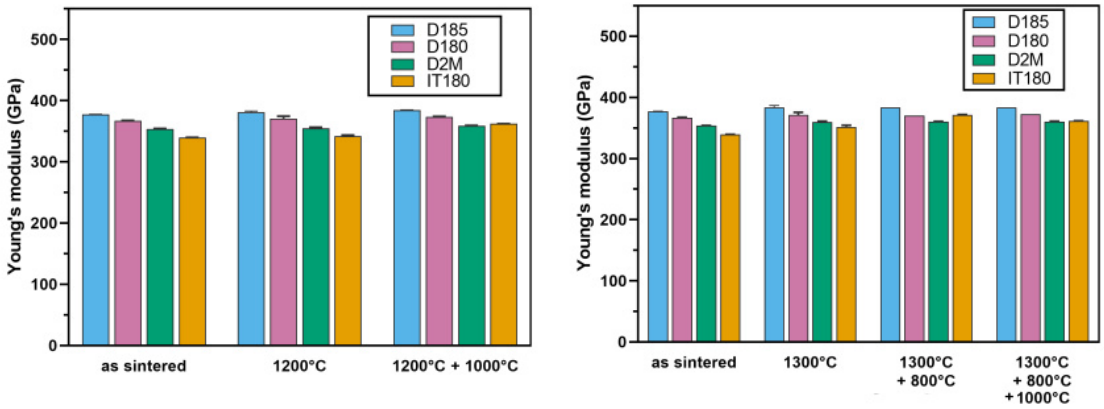

(a) **(b)**

Fig. 29: Young's modulus after consecutive heat treatment at 1200 °C for 120 h - new as-sintered state - at 1200 h for 2 h and 1000 °C for 2 h (a), 1300 °C for 120 h - new as-sintered state - at 1300 2h, 800 °C for 2 h and 1000 °C for 2 h (b)

4.1.5 Tensile test

As described in section 3.1.4 the tensile strength of materials D180 and IT180 in the as-sintered state and annealed at 1100 and 1300 °C for 2 h each was tested. In table 3 the strain and tensile strength of each sample measured are listed. Unfortunately, not all samples broke in the intended measuring range. This is why there is no value for particular samples.

Die approbierte gedruckte Originalversion dieser Diplomarbeit ist an der TU Wien Bibliothek verfügbar
The approved original version of this thesis is available in print at TU Wien Bibliothek.
TU Bibliothek Your knowledge hub WIEN

Tab. 3: Tensile tests, A=strain, σ=engineering stress

Material	**No.**	**A (%)**	$\boldsymbol{\sigma}$ **(MPa)**
D180 as-sintered	1	5.8	1072.9
	2	6.6	1073.1
	3	-	-
D180 1100 °C	1	24.2	1200.0
	2	-	-
	3	-	-
D180 1300 °C	1	17.9	1182.2
	2	19.0	1179.9
	3	19.5	1181.8
IT180 as-sintered	1	4.9	941.3
	2	4.1	934.7
	3	-	-
IT180 1100 °C	1	1.5	881.1
	2	-	-
	3	-	-
IT180 1300 °C	1	1.2	903.0
	2	-	-
	3	-	-

According to table 1, [1], the tensile strength of D185 and D180 is at 685 MPa and for IT180 it is at 800 MPa. While the measured tensile strength of material D180 in this thesis is much higher, than the value of 685 MPa, the measured value of IT180 at 1100 °C, is with a value of 881.1 MPa quite close to the value of 800 MPa, stated in [1]. Interestingly, the tensile strengths of IT180 measured at the as-sintered state as well as measured after annealing at 1300 °C are higher with a difference of about approximately 200 GPa, compared to literature [1].
In the following figures, the stress-strain diagrams are plotted. The stress-strain diagram of each sample at one temperature is put on top of each other. The numbers 1, 2 and 3 stand for the sample number.
Figure 30a, 30b and 30c show that the reproducibility is given, especially in figure 30c where all three samples could be measured. The strain increases from the as-sintered state to 1300 °C from 6.2 % to 18.8 % (the values written here are the mean values of all samples measured at one temperature). However, the mean strain of the samples annealed at 1100 °C is 24.2 %, which is higher than in the as-sintered state and also higher than the annealed samples at 1300 °C.

Die approbierte gedruckte Originalversion dieser Diplomarbeit ist an der TU Wien Bibliothek verfügbar
The approved original version of this thesis is available in print at TU Wien Bibliothek.
TU Bibliothek Your knowledge hub WIEN

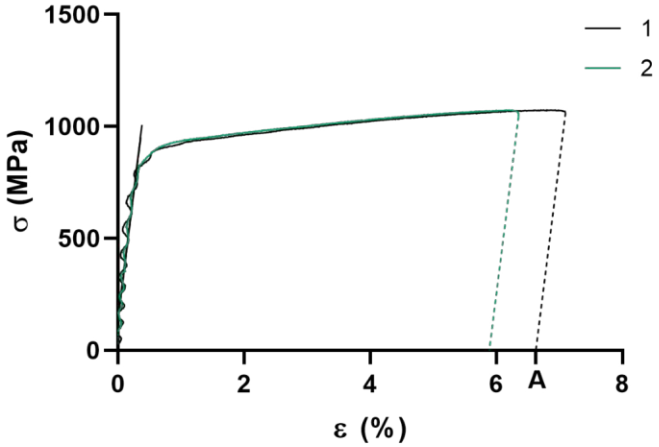

(a)

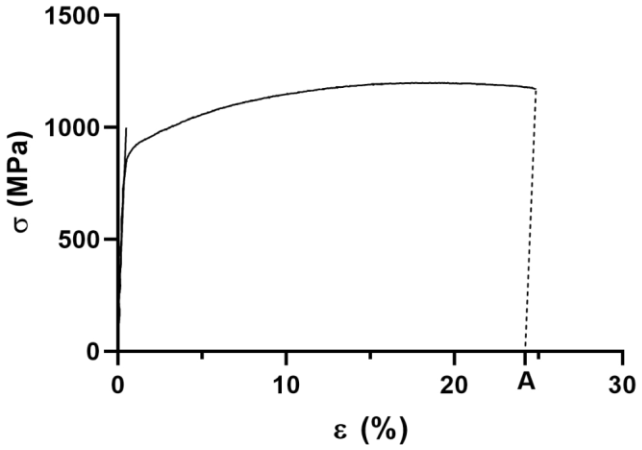

(b)

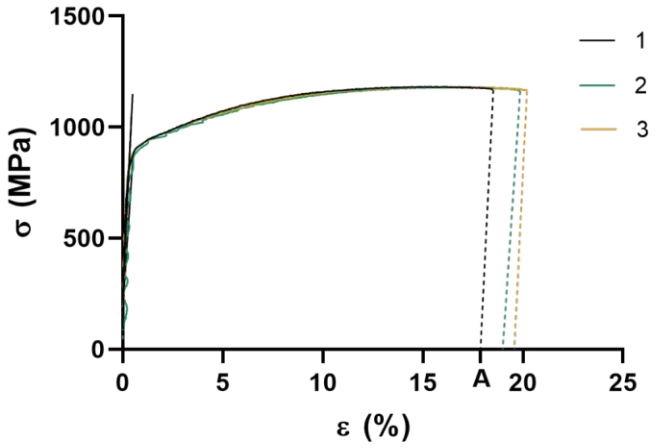

(c)

Fig. 30: Strain and tensile strength of material D180 measured at as-sintered (a), 1100 °C (b) and 1300 °C (c)

Die approbierte gedruckte Originalversion dieser Diplomarbeit ist an der TU Wien Bibliothek verfügbar
The approved original version of this thesis is available in print at TU Wien Bibliothek.

The Young's modulus can also be determined from the stress-strain diagrams. However, the calculation here is very inaccurate and therefore does not agree with the dynamically measured Young's modulus values in this thesis. The Young's modulus values determined by Hook's law are also far off the values found in literature, which is why the values of Young's modulus calculated via the stress-strain diagrams are not further discussed here.

For material IT180 the mean strain of samples in the as-sintered state is 4.5 %, see figure 31a. Then the strain decreases with samples annealed at higher temperatures, from 1.5 % at 1100 °C to 1.2 % at 1300 °C. Due to the fact, that material IT180 is very brittle, only one out of 3 samples broke in the measuring range and could be considered in the evaluation.

Die approbierte gedruckte Originalversion dieser Diplomarbeit ist an der TU Wien Bibliothek verfügbar
The approved original version of this thesis is available in print at TU Wien Bibliothek.

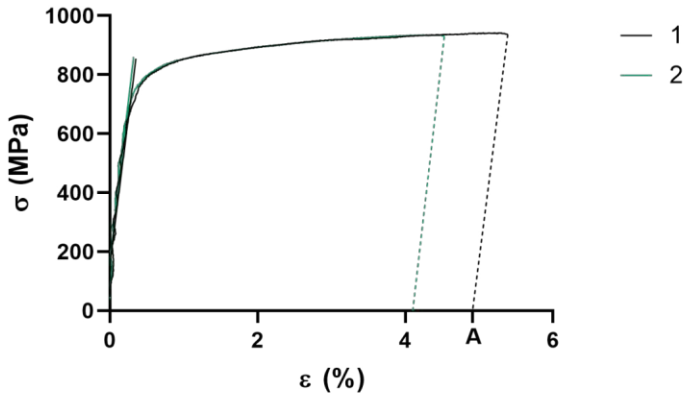

(a)

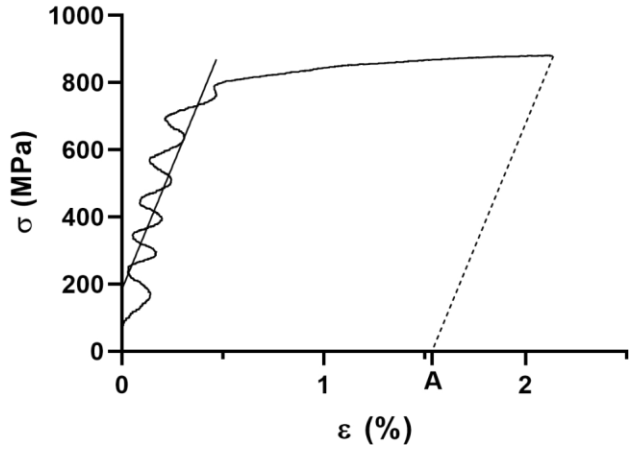

(b)

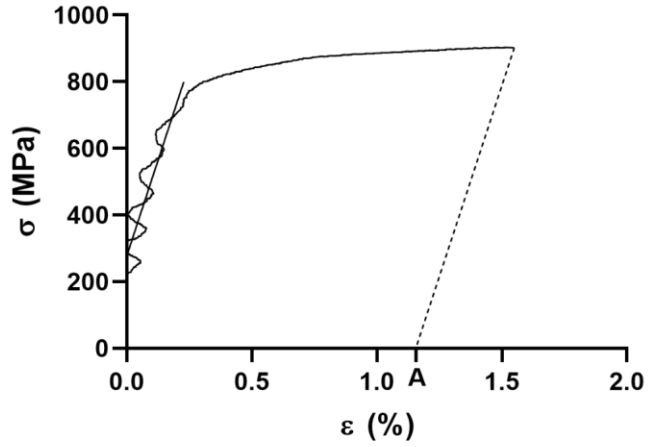

(c)

Fig. 31: Strain and tensile strength of material IT180 measured at as-sintered (a), 1100 °C (b) and 1300 °C (c)

Die approbierte gedruckte Originalversion dieser Diplomarbeit ist an der TU Wien Bibliothek verfügbar
The approved original version of this thesis is available in print at TU Wien Bibliothek.

To see the differences in the matrix of materials D180 and IT180, SEM images from fracture surfaces were taken. On the fracture surfaces below, figure 32a, 32b, delamination can be observed. Ductile fractures (green circles), so-called comb fractures, as well as brittle fractures (yellow circles) are visible on both fracture surfaces. Along the white lines, there is poor contact between tungsten particles, but also binder, indicating that pores must be involved. The purple circle in figure 32a displays a sintered contact between two tungsten particles, which might indicate poor sintering. However, in material D180 this only appears in the as-sintered state. It is suspected that the small white dots, see red arrows in figure 32a, 32b, are tungsten precipitations, since these dots appear to be heavy elements. To confirm this assumption, an EDX mapping was performed, which, unfortunately, could not provide enough information about the truth of this assumption, because the precipitates are too small and therefore too much background is measured in the EDX.

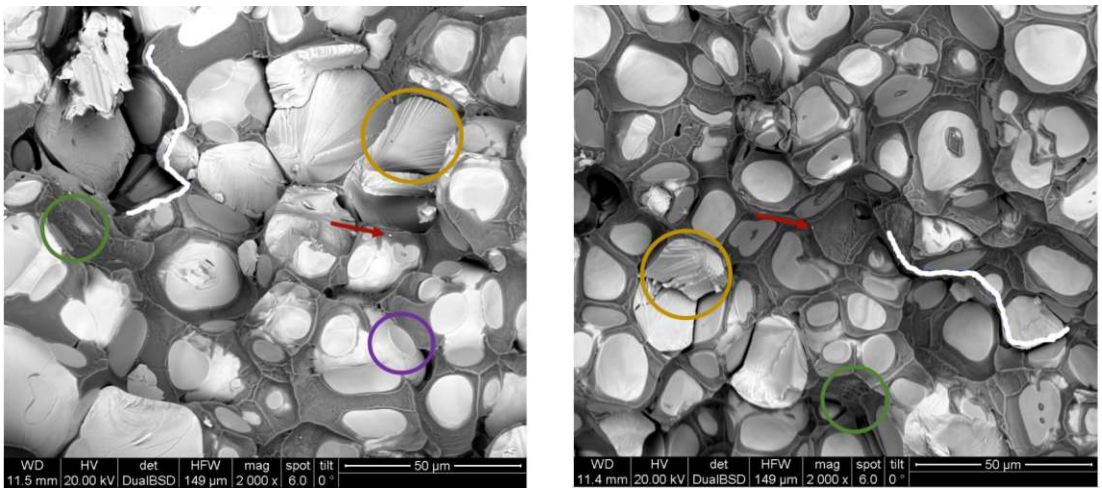

(a) **(b)**

Fig. 32: Fracture surface analysis of material D180 measured at as-sintered (a) and 1300 °C (b)

In the SEM images of material IT180 ductile and brittle fractures are also visible in the as-sintered state, see green and yellow circles in figure 33a. Precipitations are seen on the fracture surface of samples annealed at 1300 °C, see red arrow in figure 33b.
In figure 33b, along the white line, the tungsten particles as well as the matrix seem to be separated from the rest of the material. This again, indicates a porous material, where the pores might occur by the fracture itself. In material IT180, sintered contacts can be observed both in the as-sintered state and in the sample

Die approbierte gedruckte Originalversion dieser Diplomarbeit ist an der TU Wien Bibliothek verfügbar
The approved original version of this thesis is available in print at TU Wien Bibliothek.
TU Bibliothek Your knowledge hub WIEN

annealed at 1300 °C.

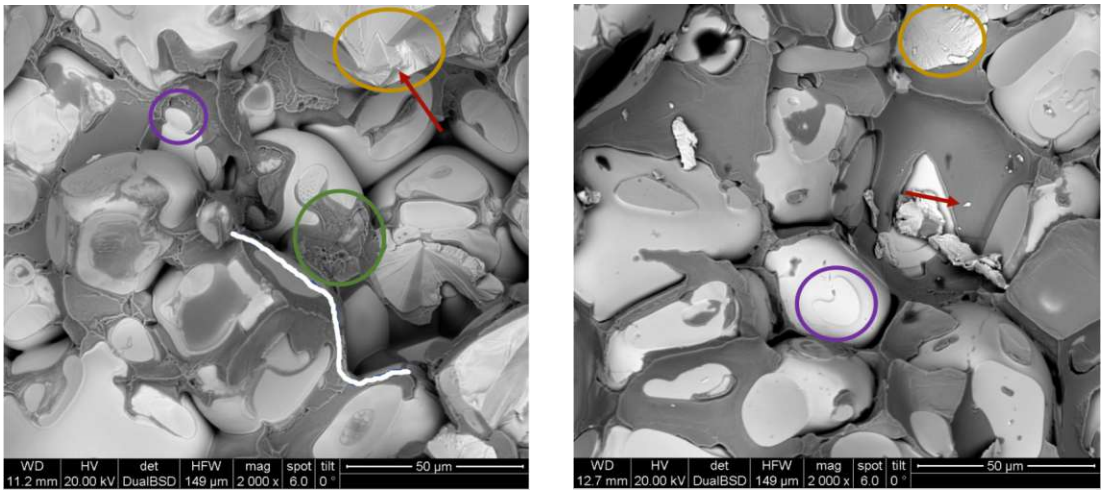

(a) **(b)**

Fig. 33: Fracture surface analysis of material IT180 measured at as-sintered (a) and 1300 °C (b)

Comparing the fracture surfaces of samples D180 and IT180, some similarities can be observed on the fracture surfaces. Both materials show ductile as well as brittle fracture behaviour. In both materials and both annealing temperatures, there is sometimes no binder to be seen between two tungsten particles. This is not due to the tensile test and indicates the poor contacts between the tungsten particles. Separated parts, that are considered pores, are also seen in every fracture surface above. Interestingly, the shapes in the purple circles are mostly discernible in IT180, especially, at an annealing temperature of 1300 °C. However, they also appear in the as-sintered state of material D180, but not when annealed at 1300 °C.
The small white dots also appear in both materials, however, mostly at an annealing temperature of 1300 °C. They are much better recognizable on the fracture surface of IT180 annealed at 1300 °C.
The most obvious difference between the fracture surfaces of materials D180 and IT180 is the particle size of tungsten. All images were taken with the same magnification. In IT180, the tungsten particles seem to be bigger, than in D180.

4.1.6 Summary of WHAs

For the measurement of the specific electrical resistivity, the thermal connectivity, the saturation magnetization and the Young's modulus, a good measuring accuracy between each measurement and reproducibility between each heat treatment

Die approbierte gedruckte Originalversion dieser Diplomarbeit ist an der TU Wien Bibliothek verfügbar
The approved original version of this thesis is available in print at TU Wien Bibliothek.
TU Bibliothek Your knowledge hub WIEN

is ensured.
Different annealing times do not change the specific electrical resistivity, significantly. Materials D185 and D180 show a decrease in specific electrical resistivity at consecutive heat treatments of firstly treated at 1200 °C for 120 h and secondly treated at 1000 °C for 2 h.
The results of measuring thermal conductivity depict differences in annealing periods. However, these differences only occur at temperatures from 1100 °C. Starting at this temperature, the thermal conductivity increases for materials D185 and IT180 when annealed for 120 h. Trying to lower the annealing time to 20 h, does not bring the anticipated results. With consecutive heat treatments, the thermal conductivity increases for all materials, compared to the specific electrical resistivity, that decreases for materials D185 and D180. Especially, for material IT180, the thermal conductivity increases with further heat treatments, starting at 1300 °C.
Similar to the specific electrical resistivity, different annealing periods do not seem to have a great impact on the saturation magnetization. In spite of that, the saturation magnetization shows changes when annealed consecutively. Comparable to the thermal conductivity, the saturation magnetization for all materials increases with consecutive heat treatments.
Material IT180 shows an exceptional behavior compared to the other materials when looking at the Young's modulus. The values for IT180 depict an increase at higher temperatures, starting at 1100 °C. Depending on the annealing period, the increase happens at a different temperature. Compared to the thermal conductivity and the saturation magnetization, the Young's modulus also increases for all 4 materials with consecutive heat treatments.

The strain of material D180 is found to be higher at samples annealed at 1100 °C than for samples annealed at 1300 °C. The strain of material IT180 is highest in the as-sintered state and decreases with higher annealing temperatures. Fracture surfaces of both materials show ductile fractures (comb fractures) as well as brittle fractures, pores and sintered contacts between two tungsten particles.

Die approbierte gedruckte Originalversion dieser Diplomarbeit ist an der TU Wien Bibliothek verfügbar
The approved original version of this thesis is available in print at TU Wien Bibliothek.
TU Bibliothek Your knowledge hub WIEN

4.2 Binder material

As the influence of heat treatments on different properties of WHAs in section 4.1 was not always easy to identify, as this might be influenced by several superimposed processes that can take place at the interfaces between the tungsten particles and the binder, or the precipitation processes in the binder alone, additional experiments were performed with the exclusion of the main fraction of tungsten. For this the binder nominal composition of D180 was chosen and additions of tungsten were realized to investigate the influence of dissolved and precipitated tungsten in the binder.
The solubility of tungsten in the matrix, analogous sample D180, was calculated with the software ThermoCalc (thermodynamic database: TCFE9), see figure 34.

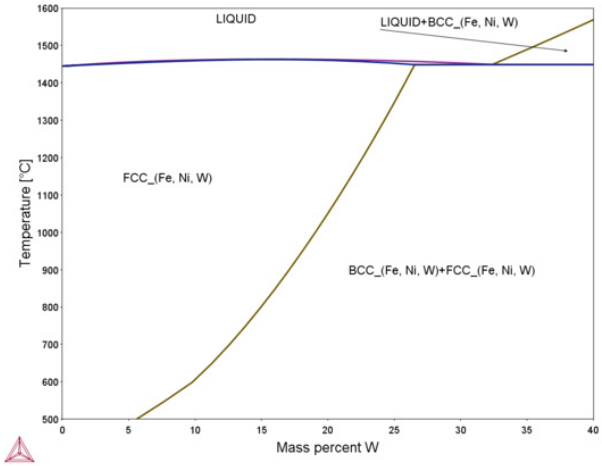

Fig. 34: Theoretical calculation of the solubility of tungsten in an iron-nickel matrix analogous sample D180 with ThermoCalc

The difference between the sample with 0 % W and 30 % W are presented in figures 35a and 35b. Both samples show high porosity, however, dense binder samples are necessary, as this is essential for the correct measurement of the physical properties, especially for the specific electrical resistivity and the thermal conductivity. Compared to 35a, in figure 35b an additional phase is discernible. This phase might most likely be elementary tungsten, that could not be dissolved.

Die approbierte gedruckte Originalversion dieser Diplomarbeit ist an der TU Wien Bibliothek verfügbar
The approved original version of this thesis is available in print at TU Wien Bibliothek.

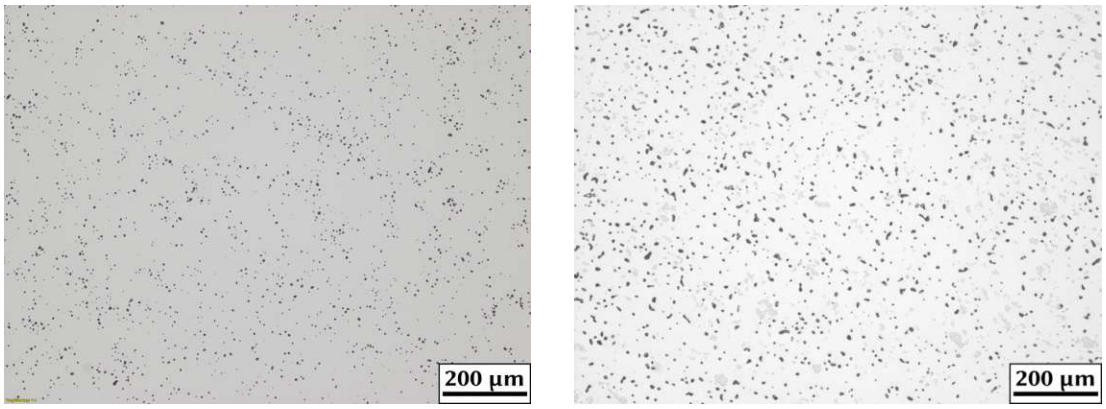

(a) **(b)**

Fig. 35: LOM images of Ni/Fe-xW binder material with 0 % W (a) and 30 % W (b) after sintering at 1400 °C

The experiments in the sinter-HIP also failed. At 1400 °C the samples melted. When those samples were cut in half, large cavities were revealed.
When looking at the phase diagram of iron-nickel, the material should not melt at 1250 °C. The temperature in the sinter-HIP was then reduced to 1250 °C for a new run. But after sintering at this lower temperature, not much has changed, as the samples were still very porous, figure 36.

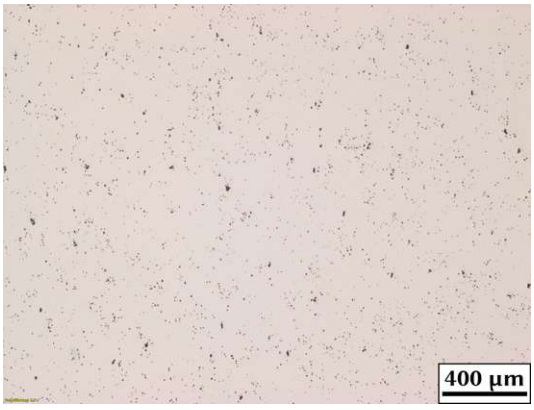

Fig. 36: Ni/Fe-xW binder material with 0 % tungsten content after sinter-HIP at 1250 °C

4.2.1 DTA

Due to the failed attempts described in section 4.2, the information of the exact melting point of the binder material was required. Accordingly, differential thermal analysis was used, as described in section 3.3.7. The result shows, that the melting point of the binder material is at 1492.6 °C, see figure 37. The binder material

Die approbierte gedruckte Originalversion dieser Diplomarbeit ist an der TU Wien Bibliothek verfügbar
The approved original version of this thesis is available in print at TU Wien Bibliothek.

starts melting at 1478 °C, therefore it is yet unclear, why the samples melted in the sinter-HIP at a temperature of 1400 °C.

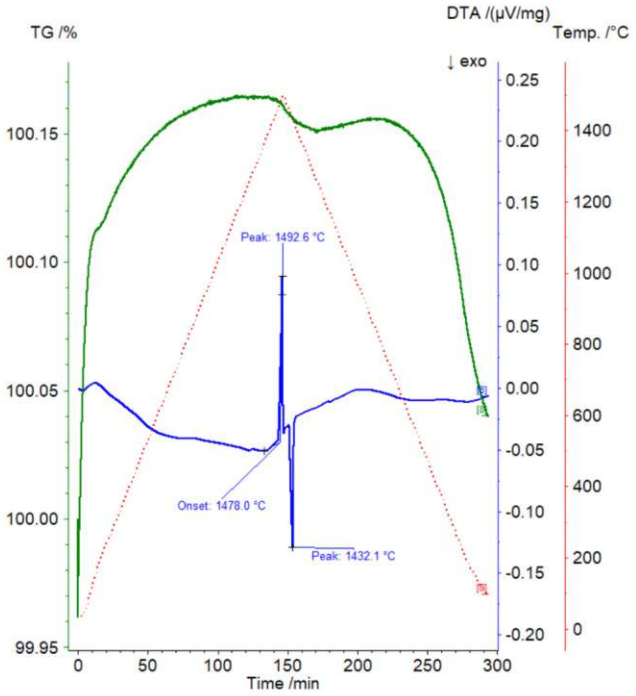

Fig. 37: DTA measurement

4.2.2 Hot extrusion

Subsequently, a new approach by powder hot extrusion was tried to eliminate the porosity of the samples, as described in section 3.2.3.
Since it was assumed that hot extrusion alone would not dissolve tungsten in the binder, subsequent heat treatment was carried out after extrusion. Firstly, a dissolution heat treatment step was executed with the binder materials at 1250 °C for 72 h. This step was from now on considered as an apparent as-sintered state. Precipitation heat treatments at 1300, 1000 and 800 °C for 2 h each, followed.
The hot extrusion for the sample with 10 % tungsten did not work as all other samples, as parameters had first to be adjusted and led to a very limited size of the extruded rod (8 x 30 mm). Therefore only LOM and SEM images of the 3 other samples are shown in the following.
After the 72 h dissolution heat treatment at 1250 °C, a subsequent precipitation heat treatment was started, similar to the ones described in section 4.1. Firstly, the samples were annealed at 1300 °C for 2 h. Note, that the total number of heat treatment operations for the hot extruded samples is limited, as the total

Die approbierte gedruckte Originalversion dieser Diplomarbeit ist an der TU Wien Bibliothek verfügbar
The approved original version of this thesis is available in print at TU Wien Bibliothek.

length of the extruded rods is limited. Thus, only selected consecutive heat treatment schemes could be applied. The LOM images after this considered first heat treatment are shown in the following figure.

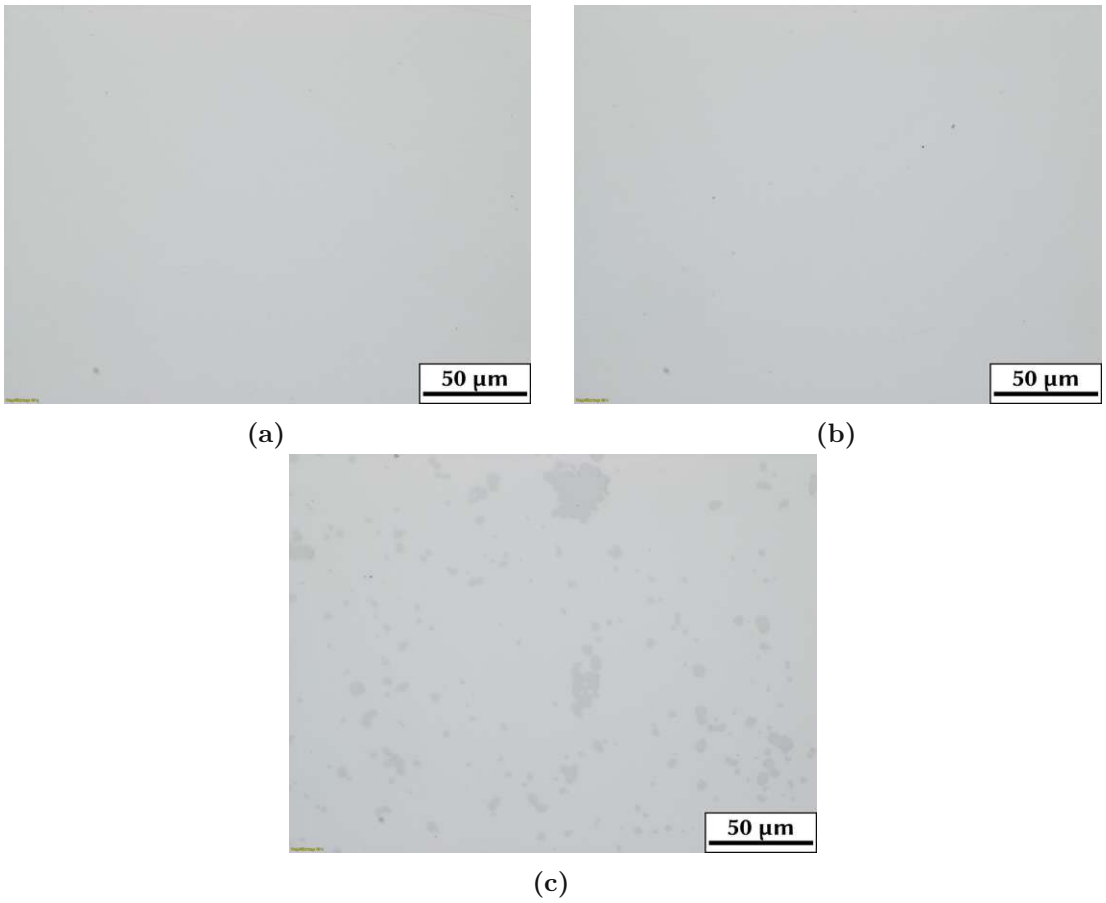

(a) **(b)**

(c)

Fig. 38: LOM images of hot extruded NiFe/-xW binder with 0 % W (a), 20 % W (b), 30 % W (c) content after dissolution heat treatment at 1250 °C for 72 h and precipitation heat treatment at 1300 °C for 2 h

No differences can be seen between 0 and 20 % tungsten content. In both LOM images only one phase is visible. This means, that the 20 % tungsten content must be fully dissolved in the nickel-iron matrix. In the LOM image of 30 % tungsten content, another phase can now be recognized. This might be not-dissolved tungsten, see figure 34.

Die approbierte gedruckte Originalversion dieser Diplomarbeit ist an der TU Wien Bibliothek verfügbar
The approved original version of this thesis is available in print at TU Wien Bibliothek.

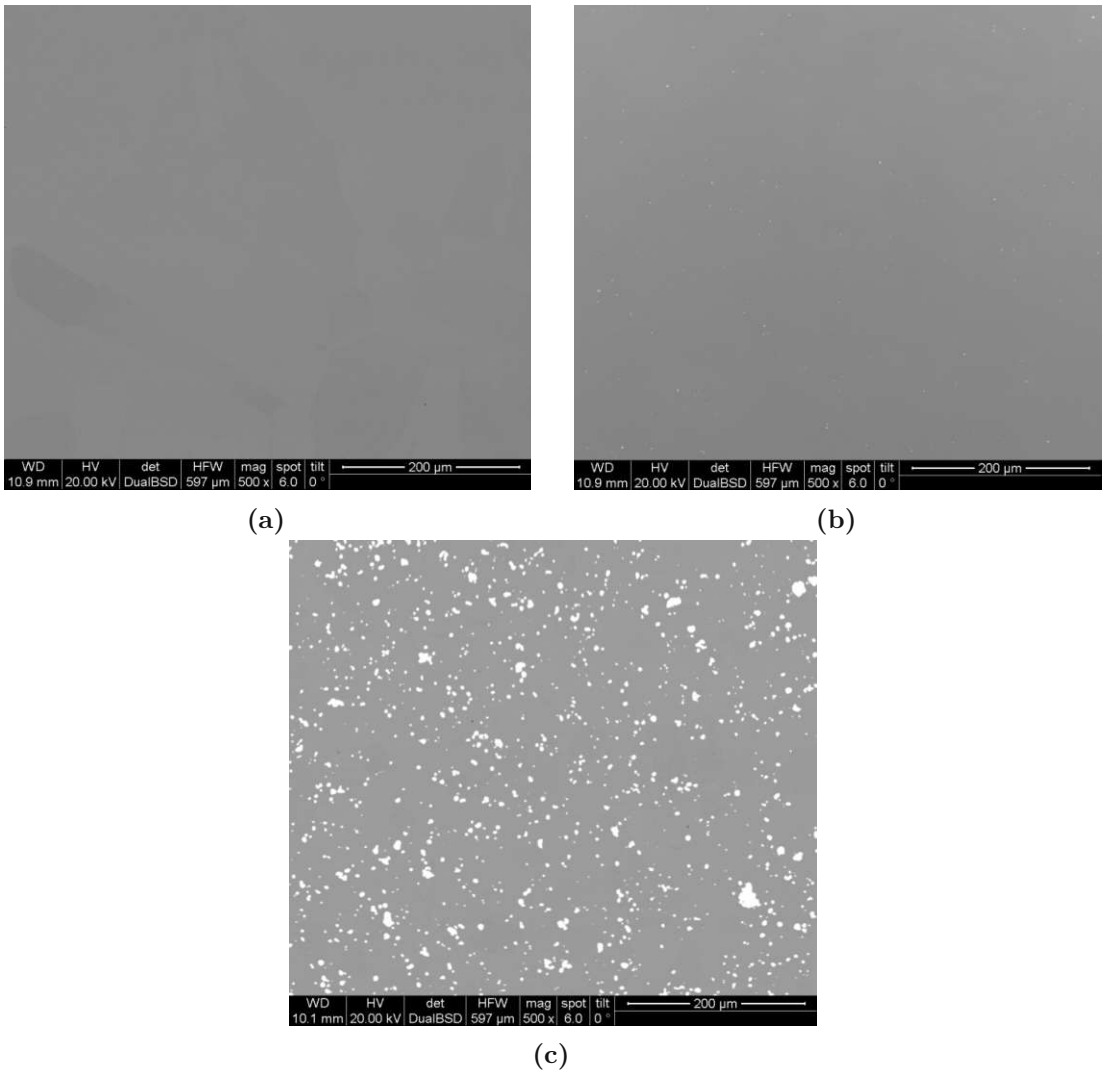

Fig. 39: SEM images of hot extruded NiFe/-xW binder with 0 % W (a), 20 % W (b), 30 % W (c) content after dissolution heat treatment at 1250 °C for 72 h and precipitation heat treatment at 1300 °C for 2 h

Figure 39a shows a uniform structure of the nickel-iron matrix, which coincides with the LOM images above, figure 39a. In figure 39b very few scattered white particles are visible. An EDX analysis shows, that those particles are most probably tungsten. In the binder material with 30 % W content, figure 39c, many of those tungsten particles are visible throughout the whole sample. This also fits to the LOM image, see figure 39c. This could well be true, since the theoretical solubility of tungsten in an iron-nickel binder is around 27.5 %, figure 34. The sample with 30 % tungsten content has already exceeded this value, which is why no more tungsten can be dissolved [25].

Die approbierte gedruckte Originalversion dieser Diplomarbeit ist an der TU Wien Bibliothek verfügbar
The approved original version of this thesis is available in print at TU Wien Bibliothek.
TU Bibliothek Your knowledge hub WIEN

An EDX mapping of both samples, 20 % and 30 % tungsten content, shows, that tungsten is also found in the binder. Consequently, tungsten is at least partly dissolved.

Next, the same binder materials were annealed at 1000 °C, figure 40a, 40b, 40c and finally at 800 °C for 2 h each, 41a, 41b, 41c.

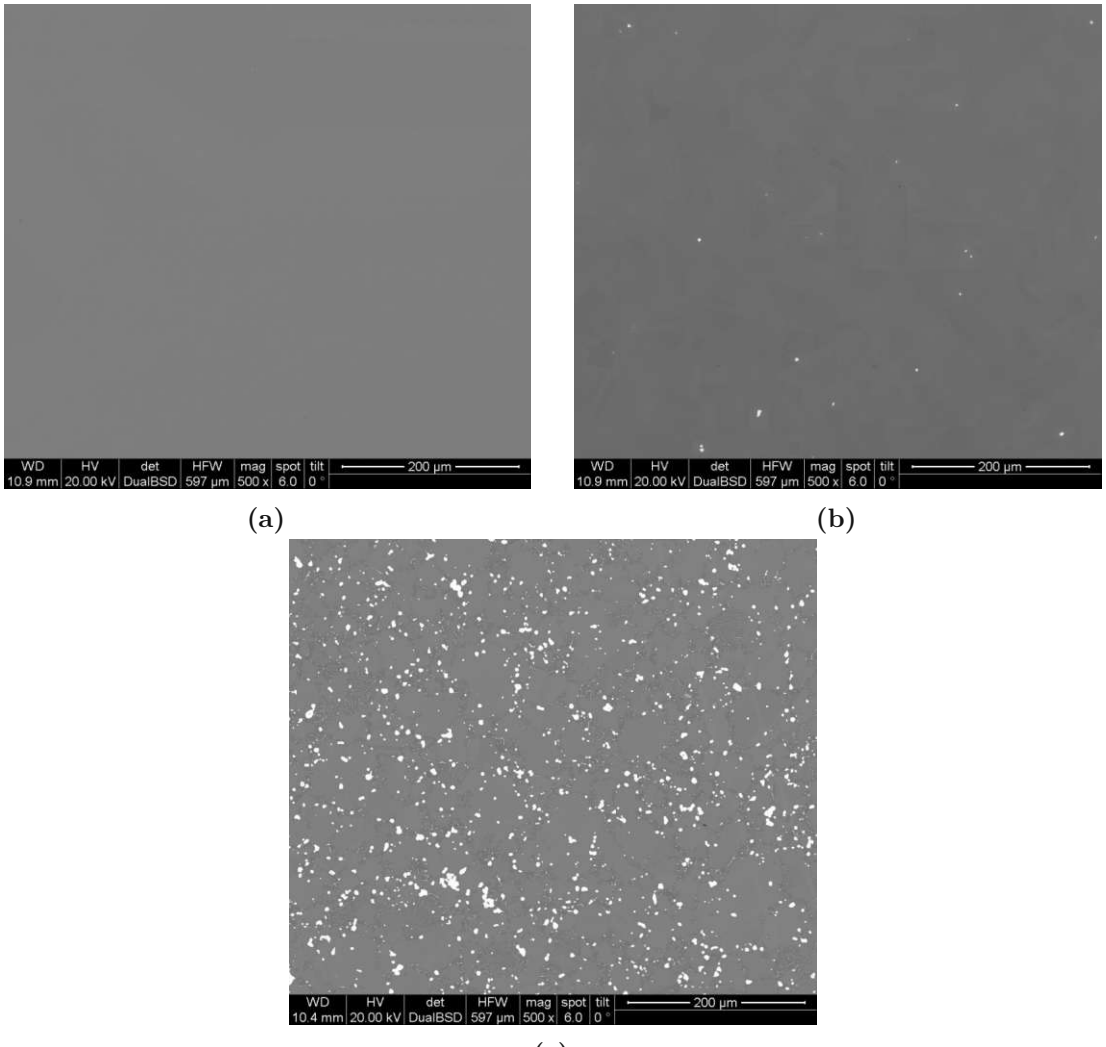

(a) **(b)**

(c)

Fig. 40: SEM images of hot extruded NiFe/-xW binder with 0 % W (a), 20 % W (b), 30 % W (c) content after dissolution heat treatment at 1250 °C for 72 h and precipitation heat treatments at 1300 °C and at 1000 °C for 2 h each.

The SEM images of the samples annealed at 1300 °C first and then at 1000 °C, 40a, 40b and 40c, look similar to the samples only annealed at 1300 °C. EDX also

Die approbierte gedruckte Originalversion dieser Diplomarbeit ist an der TU Wien Bibliothek verfügbar
The approved original version of this thesis is available in print at TU Wien Bibliothek.
TU Bibliothek Your knowledge hub WIEN

shows, that tungsten is existent in the binder matrix of samples with 20 % and 30 % tungsten content.

The SEM images of the samples annealed firstly at 1300 °C, then at 1000 °C and finally at 800 °C, 41a, 41b and 41c, are similar to the the SEM images above. The content of tungsten particles which is visible in the sample with 20 % tungsten content, seems to be slightly lower than in previous heat treatments.
In figure 41c not only round tungsten particles as in the images above are noticeable, but also more agglomerates of tungsten particles.

Die approbierte gedruckte Originalversion dieser Diplomarbeit ist an der TU Wien Bibliothek verfügbar
The approved original version of this thesis is available in print at TU Wien Bibliothek.

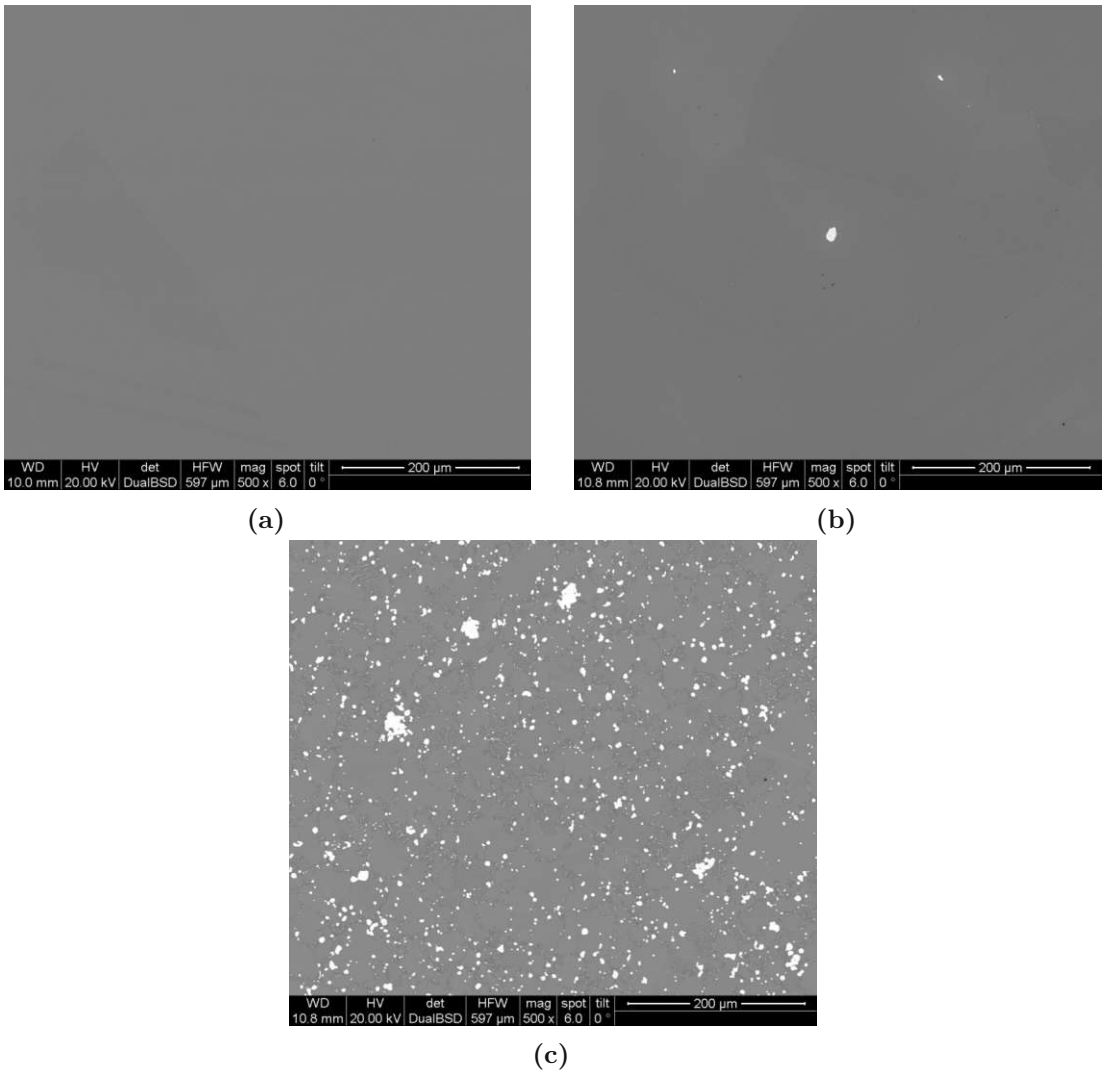

(a) **(b)**

(c)

Fig. 41: SEM images of hot extruded NiFe/-xW binder with 0 % W (a), 20 % W (b), 30 % W (c) content after dissolution heat treatment at 1250 °C for 72 h and precipitation heat treatments at 1300 °C, 1000 °C and 800 °C for 2 h each.

When increasing the magnification on the SEM image 41c, details of the microstructure of NiFe-30W are visible. The tungsten particles are mainly located at the grain boundaries and also white, elongated phases appear also mainly at the grain boundaries. Furthermore, a darker phase besides the nickel-iron phase is observable. The material now seems to have 3 phases, see figure 42a. To determine this phase, an EDX mapping, figure 42b, was executed. Unfortunately, the phase is not observable in the EDX mapping, which is why, an XRD analysis was performed.

Die approbierte gedruckte Originalversion dieser Diplomarbeit ist an der TU Wien Bibliothek verfügbar
The approved original version of this thesis is available in print at TU Wien Bibliothek.
TU Bibliothek Your knowledge hub WIEN

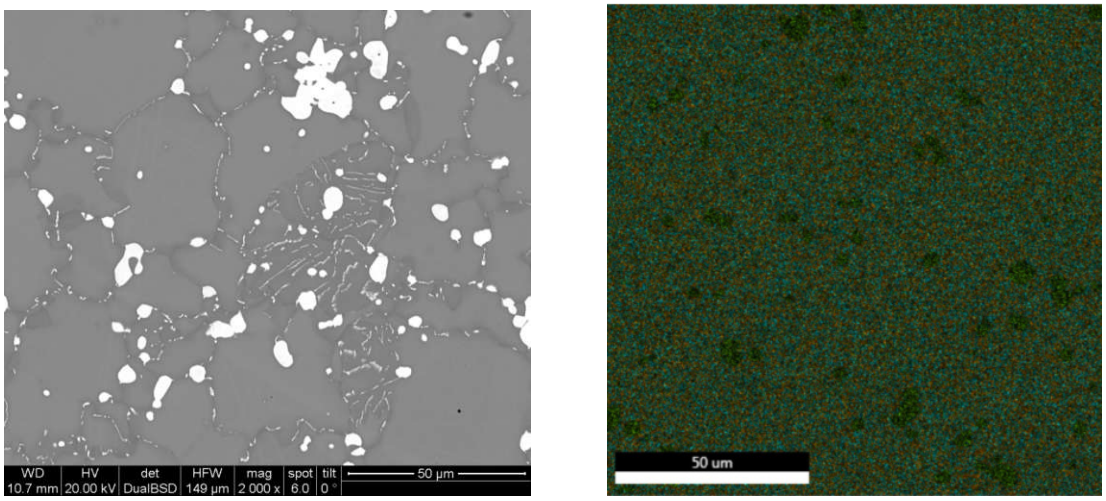

(a) **(b)**

Fig. 42: SEM image (a) and EDX mapping (b) of hot extruded NiFe-30 % W binder after dissolution heat treatment at 1250 °C for 72 h and precipitation heat treatments at 1300 °C, 1000 °C and 800 °C for 2 h each (blue: Fe, orange: Ni, green: W)

XRD of the sample with 0 % and 20 % W only shows one phase, the iron-nickel phase, see figure 43a and 43b. This implies, that tungsten is fully dissolved in the matrix or that the precipitations are too small to be identified in the XRD. When considering the binder material with 30 %, figure 43c, tungsten is visible as an additional single phase. This observation fits to the SEM images, since for this binder composition there are many tungsten particles seen throughout the whole sample. The lattice parameters increase with higher tungsten content and moreover increase slightly between the different heat treatments, see table 4.

Tab. 4: Lattice parameters of different heat treatments of hot extruded NiFe/-xW binder after dissolution heat treatment at 1250 °C for 72 h

	1300 °C, 2 h	1300 °C, 2 h + 1000 °C, 2 h	1300 °C, 2 h + 1000 °C, 2 h + 800 °C, 2h	
	FeNi lattice parameter [Å]	FeNi lattice parameter [Å]	FeNi lattice parameter [Å]	W lattice parameter [Å]
0 % W	3.55	3.56	3.56	
20 % W	3.58	3.58	3.57	
30 % W	3.58	3.59	3.60	3.17

Figure 44a, 44b and 44c show diffractograms of the binder materials after the final consecutive heat treatment. Again, in the samples with 0 % and 20 % W content only the iron-nickel phase is visible. In figure 44c, an additional tungsten phase is found beside the iron-nickel phase. Furthermore, as discussed on the

Die approbierte gedruckte Originalversion dieser Diplomarbeit ist an der TU Wien Bibliothek verfügbar
The approved original version of this thesis is available in print at TU Wien Bibliothek.
TU Bibliothek Your knowledge hub WIEN

basis of the SEM images above, a third phase was identified. Unfortunately, these reflexes could not be clearly assigned to any structures in the database.

Die approbierte gedruckte Originalversion dieser Diplomarbeit ist an der TU Wien Bibliothek verfügbar
The approved original version of this thesis is available in print at TU Wien Bibliothek.
TU Bibliothek Your knowledge hub WIEN

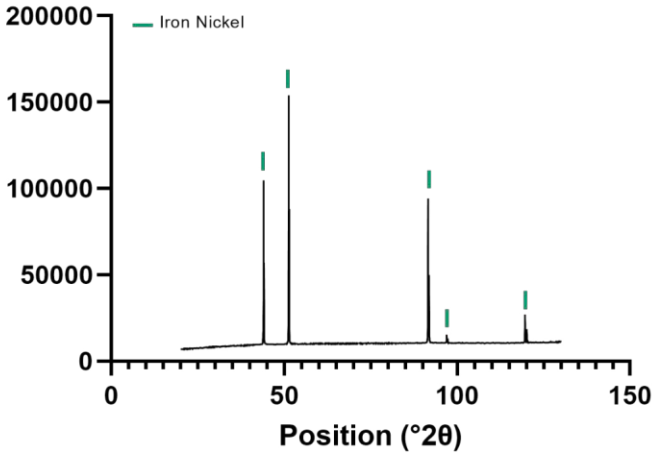

(a)

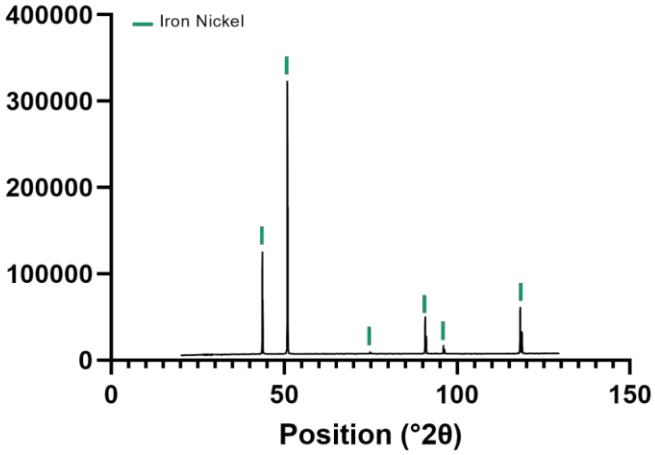

(b)

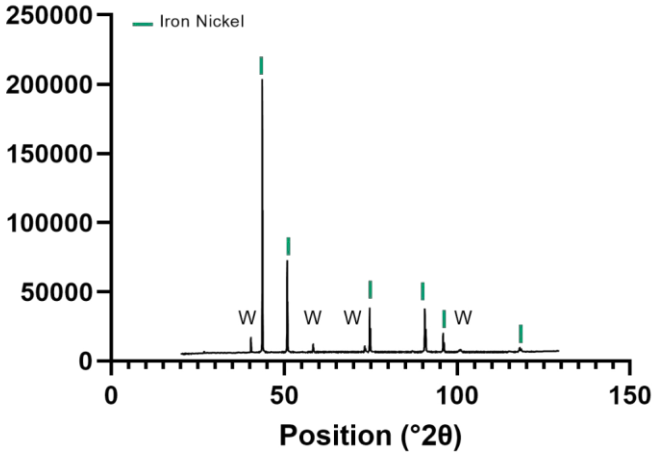

(c)

Fig. 43: XRD analysis of hot extruded NiFe/-xW binder material with 0 % W (a), 20 % W (b) and 30 % W (c) content after dissolution heat treatment at 1250 °C for 72 h and precipitation heat treatments at 1300 °C for 2 h.

Die approbierte gedruckte Originalversion dieser Diplomarbeit ist an der TU Wien Bibliothek verfügbar
The approved original version of this thesis is available in print at TU Wien Bibliothek.

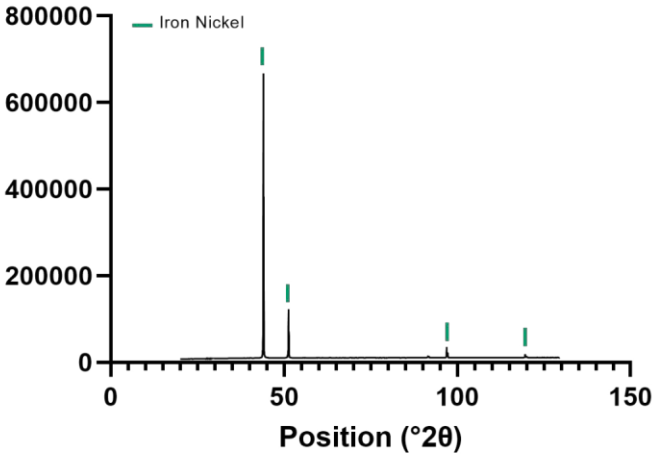

(a)

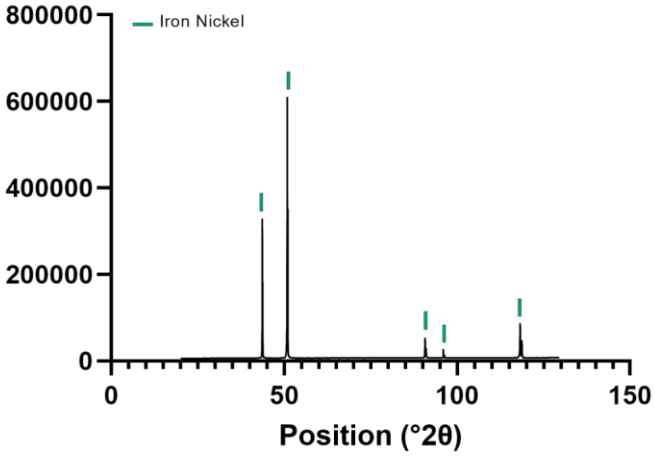

(b)

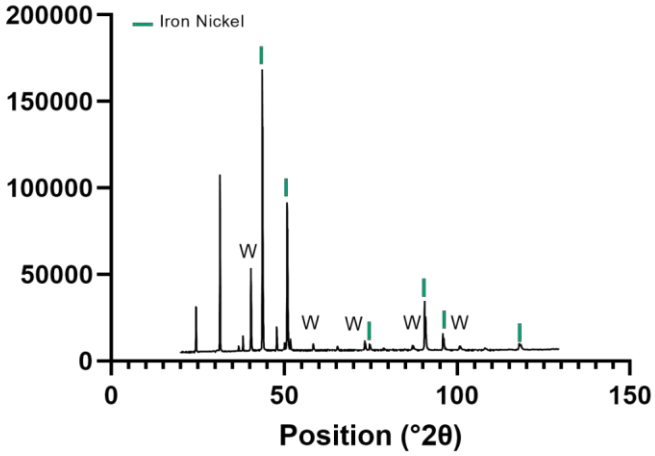

(c)

Fig. 44: XRD analysis of hot extruded NiFe/-xW binder material with 0 % W (a), 20 % W (b) and 30 % W (c) content after dissolution heat treatment at 1250 °C for 72 h and precipitation heat treatments at 1300 °C, 1000 °C and 800 °C for 2 h each

Die approbierte gedruckte Originalversion dieser Diplomarbeit ist an der TU Wien Bibliothek verfügbar
The approved original version of this thesis is available in print at TU Wien Bibliothek.

4.2.3 Specific electrical resistivity

As mentioned above, after each heat treatment the four properties - specific electrical resistivity, thermal conductivity, saturation magnetization and Young's modulus - were measured on the binder materials. Starting with the specific electrical resistivity, figure 45a, an increases with higher tungsten content is observable.

To see the changes in specific electrical resistivity more clearly, the values of each material are displayed separately in figure 45b. The specific electrical resistivity for materials with 0 and 30 % tungsten content remains almost constant, while the specific electrical resistivity for materials with 10 and 20 % decrease with consecutive heat treatments. The specific electrical resistivity for material 20 % increases after the second heat treatment and decreases with the following heat treatments.

The decrease of the specific electrical resistivity of the binder materials here fits to the decrease of the specific electrical resistivity with consecutive heat treatments of WHAs, section 4.1.1.

Die approbierte gedruckte Originalversion dieser Diplomarbeit ist an der TU Wien Bibliothek verfügbar
The approved original version of this thesis is available in print at TU Wien Bibliothek.
TU Bibliothek Your knowledge hub WIEN

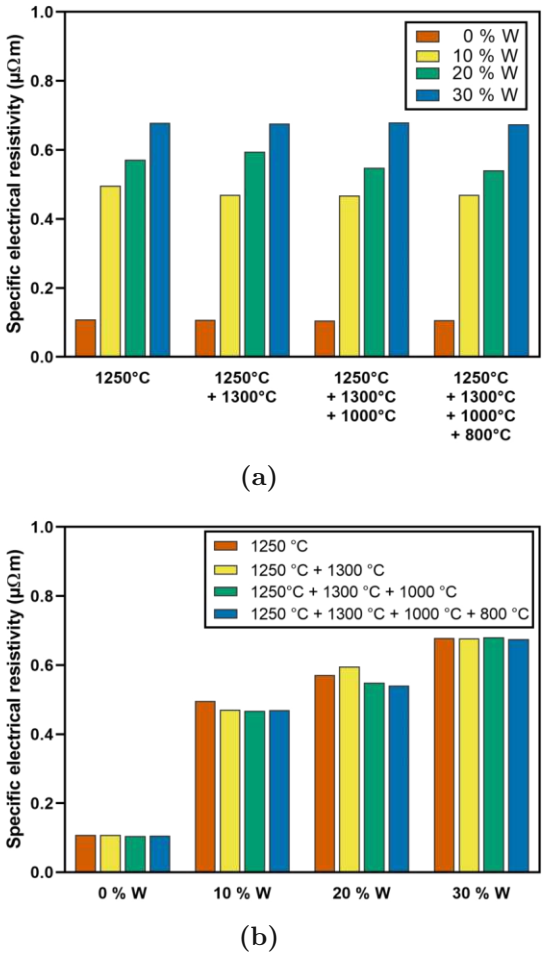

Fig. 45: Specific electrical resistivity of hot extruded NiFe/-xW binder materials with 0, 10, 20 and 30 % W content after dissolution heat treatment at 1250 °C for 72 h and precipitation heat treatment at 1300 °C, at 1000 °C and at 800 °C for 2 h each

4.2.4 Thermal conductivity

In this context, the influence of the binder can be well understood. Tungsten has a high thermal conductivity and in a naive picture one would expect an increase in thermal conductivity with increasing tungsten content. However, due to the fact, that tungsten is mostly dissolved in the Ni-Fe binder, a decrease in thermal conductivity is more likely. This is confirmed by the results in figure 46a.
While the thermal conductivity stays almost constant for the binder materials with 0 and 10 % tungsten content with consecutive heat treatments, it increases in the binder material with 20 % tungsten, figure 46b. Contrary to that, the thermal conductivity of the binder material with 30 % tungsten decreases with consecutive

Die approbierte gedruckte Originalversion dieser Diplomarbeit ist an der TU Wien Bibliothek verfügbar
The approved original version of this thesis is available in print at TU Wien Bibliothek.
TU Bibliothek Your knowledge hub WIEN

heat treatments.
Figures 19a and 19b show similar behaviour as for D180, the thermal conductivity increases with consecutive heat treatment.

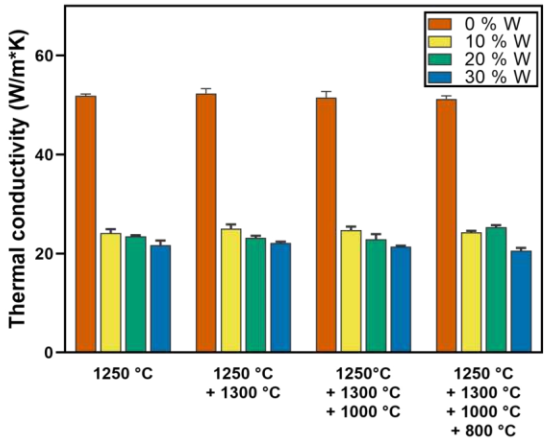

(a)

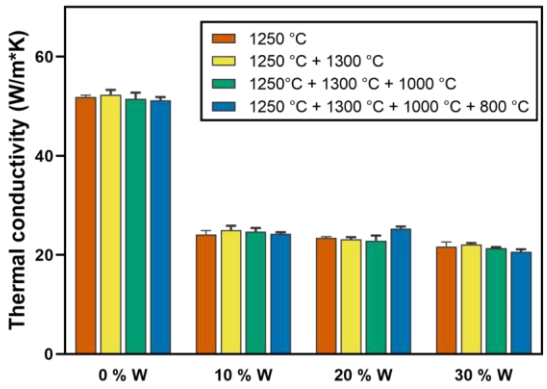

(b)

Fig. 46: Thermal conductivity of hot extruded binder NiFe/-xW materials with 0, 10, 20 and 30 % W content after dissolution heat treatment at 1250 °C for 72 h and precipitation heat treatment at 1300 °C, at 1000 °C and at 800 °C for 2 h each

4.2.5 Saturation magnetization

With increasing tungsten content, the saturation magnetization decreases, see figure 47a. Interestingly, at a tungsten content of 30 %, the saturation magnetization is higher than in the FeNi-20 % W binder, figure 47b. With respect to the heat treatments, binder materials with 20 and 30 % tungsten content increase with consecutive heat treatments, while materials with 0 and 10 % tungsten content remain almost constant.

Die approbierte gedruckte Originalversion dieser Diplomarbeit ist an der TU Wien Bibliothek verfügbar
The approved original version of this thesis is available in print at TU Wien Bibliothek.
TU Bibliothek Your knowledge hub WIEN

This correlation fits the saturation magnetization of the WHA samples with consecutive heat treatments in section 4.1.3. The saturation magnetization of WHAs also increases with consecutive heat treatments.

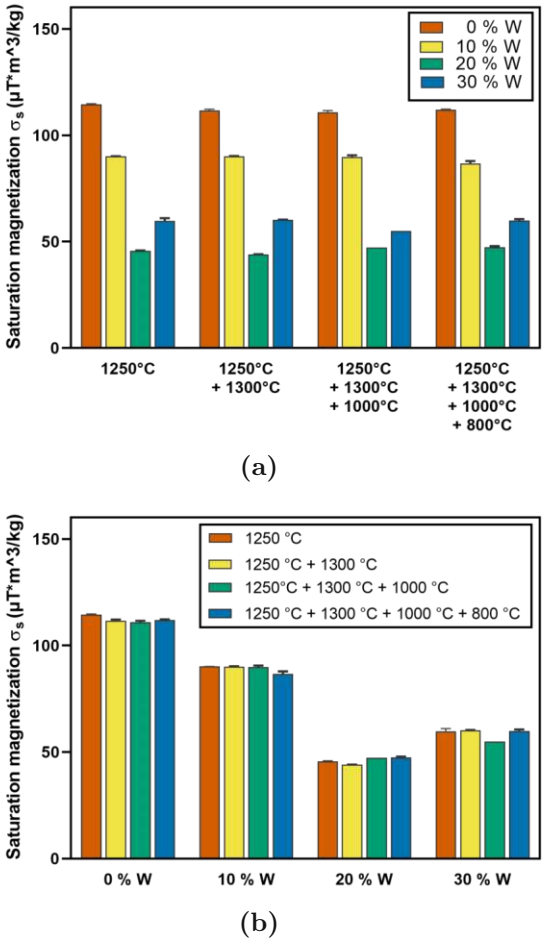

Fig. 47: Saturation magnetization of hot extruded NiFe/-xW binder materials with 0, 10, 20 and 30 % W content after dissolution heat treatment at 1250 °C for 72 h and precipitation heat treatment at 1300 °C, at 1000 °C and at 800 °C for 2 h each

4.2.6 Low-temperature measurements

Important to mention here, is, that the samples for low-temperature measurements are not heat-treated, but as-cast, unlike the samples discussed previously.

Die approbierte gedruckte Originalversion dieser Diplomarbeit ist an der TU Wien Bibliothek verfügbar
The approved original version of this thesis is available in print at TU Wien Bibliothek.
TU Bibliothek Your knowledge hub WIEN

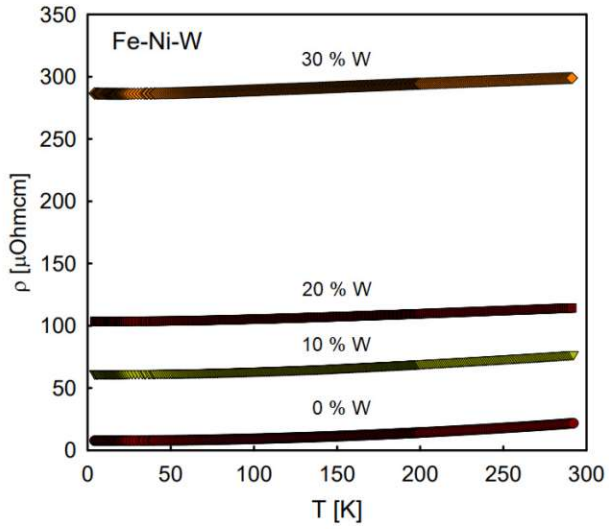

(a)

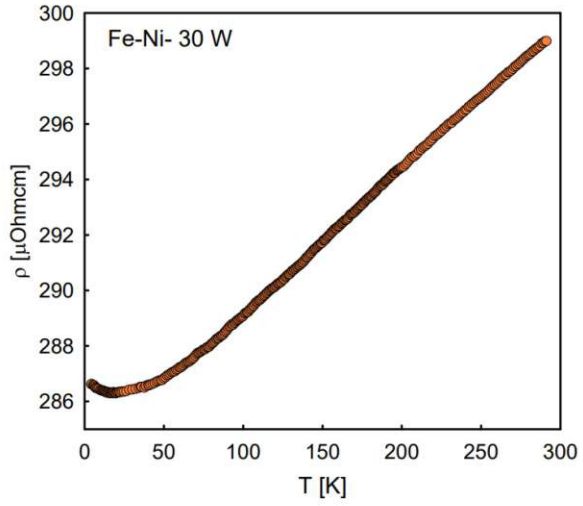

(b)

Fig. 48: Electrical resistivity of inductively melted NiFe/-xW samples with 0, 10, 20 and 30 % tungsten content (a) and of sample FeNi-30 % W (b) measured from 4.2 to 293 K.

Figure 48a depicts a higher electrical conductivity with increasing tungsten content and with increasing temperature. This can be attributed to increasing disorder in the lattice with increasing tungsten content. Moreover, FeNi-30 W shows an interesting temperature dependent behaviour, as there is a minimum in the low temperature region, figure 48b. Since the Kondo effect cannot exist due to the ferromagnetic state, this should be a sign of localisation of the charge

Die approbierte gedruckte Originalversion dieser Diplomarbeit ist an der TU Wien Bibliothek verfügbar
The approved original version of this thesis is available in print at TU Wien Bibliothek.

carriers (due to the disorder in lattice). While the samples with 0, 10 and 20 % tungsten show an electrical conductivity between 7 and 115 $\mu Ohmcm$, the electrical conductivity of the 30 % tungsten sample reaches up to 299 $\mu Ohmcm$. The huge gap difference between 20 % and 30 % is interesting.

Figure 49 displays the standardized electrical resistivity ρ/ρ_{300K}. A least square fit of FeNi-0 % W with the model of a ferromagnetic ground state (T^2 behaviour) fits perfectly in the whole temperature range (yellow line $\rho = \rho_0 + kT^2$).

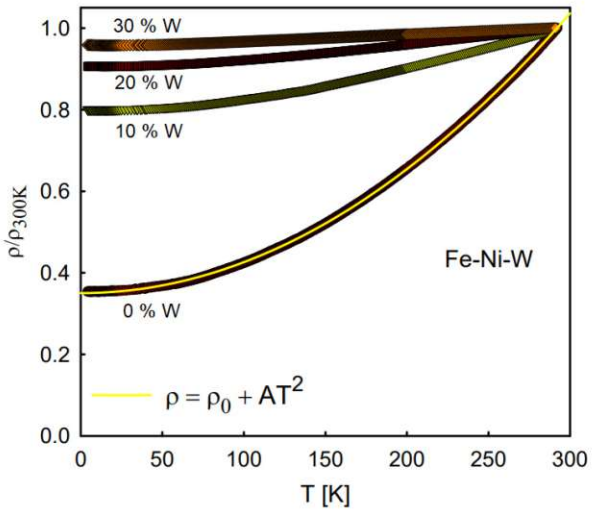

Fig. 49: Electrical resistivity of inductively melted NiFe/-xW samples measured from 4.2 to 293 K.

In table 5, the RRR values, calculated with equation 5, for each sample are represented. It shows, that with higher tungsten content, the RRR value, hence, the purity, decreases. This can be also deduced from the standardized representation in figure 49.

Tab. 5: Calculated RRR values of inductively melted NiFe/-xW samples

	0 % W	**10 % W**	**20 % W**	**30 % W**
RRR	2.6	1.2	1.1	1.0

The Wiedemann-Franz law was calculated with equation 3 using the electrical conductivity values at room temperature from the low-temperature experiments. The results are shown in table 6. The resulting values for thermal conductivity were compared to the measured thermal conductivity after consecutive heat treatments,

Die approbierte gedruckte Originalversion dieser Diplomarbeit ist an der TU Wien Bibliothek verfügbar
The approved original version of this thesis is available in print at TU Wien Bibliothek.
TU Bibliothek Your knowledge hub WIEN

figure 46a. The correlation between the thermal and electrical conductivity is given for the sample with 30 % tungsten content. However, for all other samples, the calculated thermal conductivity does not match the thermal conductivity measured in section 4.1.2.

Tab. 6: Comparison of the calculated and measured thermal conductivity at room temperature

	0 % W	**10 % W**	**20 % W**	**30 % W**
calculated λ (W/m*K)	1	5	8	22
measured λ (W/m*K)	51	24	25	20

The absolute values of the specific electrical resistivity of FeNi/-xW binder materials depicted in figure 48a at ambient temperature are compared to the hot extruded FeNi/-xW binder materials, displayed in figure 45a, after dissolution heat treatment at 1250 °C for 72 h and precipitation heat treatment at 1300 °C, at 1000 °C and at 800 °C for 2 h each in table 7. The specific electrical resistivity of the absolute values is for all materials higher than the specific electrical resistivity of the hot extruded binder materials. While the difference between the two samples with 0 % tungsten content seems to be quite low with 0.11 μOhmm, the difference between the two samples with 30 % tungsten content is with a value of 2.32 μOhmm more significant.

Tab. 7: Comparison of the specific electrical resistivity of the absolute values of FeNi/-xW measured at ambient temperature and the specific electrical resistivity of the hot extruded FeNi/-xW binder materials after dissolution heat treatment at 1250 °C for 72 h and precipitation heat treatment at 1300 °C, at 1000 °C and at 800 °C for 2 h each.

	0 % **W**	10 % **W**	20 % **W**	30 % **W**
specific electrical resistivity of absolute values (μOhmm)	0.22	0.77	1.14	2.99
specific electrical resistivity of hot extruded binder (μOhmm)	0.11	0.47	0.54	0.67

4.2.7 Summary binder materials

Since the influence of different heat treatments on the properties of WHAs was rather difficult to distinguish, experiments without the main fraction of tungsten were executed. Hot extrusion and subsequent heat treatments make good methods to produce these non-porous binder materials. Tungsten was found to be mostly dissolved in the binder, with the binder material FeNi-30 % W being an exception as many unsolved tungsten particles are visible in the SEM images, as well as a

Die approbierte gedruckte Originalversion dieser Diplomarbeit ist an der TU Wien Bibliothek verfügbar
The approved original version of this thesis is available in print at TU Wien Bibliothek.

new separate phase. However, this phase could not be identified with an XRD analysis.

The properties of the binder material were measured in order to determine the influence of the binder itself, without the high tungsten content. Unfortunately, the changes of the properties in the binder materials, are quite small and no significant conclusion can be drawn from it. Moreover, the changes of properties in the binder material mostly fit to the changes in WHAs. This gives the impression that the binder itself has no significant influence.

The electrical conductivity at low-temperature measurements is higher with increasing tungsten content and with increasing temperature. Ni-30 W shows an interesting temperature dependent behaviour, as there is a minimum in the low temperature region. The RRR value decreases with increasing tungsten content. The calculated thermal conductivity does not match the thermal conductivity measured in this thesis. The comparison of the specific electrical resistivity of the absolute values measured at ambient temperature and the specific electrical resistivity of the hot extruded FeNi/-xW binder materials after dissolution heat treatment at 1250 °C for 72 h and precipitation heat treatment at 1300 °C, at 1000 °C and at 800 °C for 2 h each, exposes significant differences.

Die approbierte gedruckte Originalversion dieser Diplomarbeit ist an der TU Wien Bibliothek verfügbar
The approved original version of this thesis is available in print at TU Wien Bibliothek.
TU Bibliothek Your knowledge hub WIEN

5 Summary and outlook

The improvement of the 4 properties, specific electrical resistivity, thermal conductivity, saturation magnetization and Young's modulus, was to be achieved by various heat treatments. However, this could only be successfully accomplished for individual materials.
The specific electrical resistivity could not be influenced despite annealing times of different lengths. However, with consecutive heat treatments, materials D185 and D180 show a decrease in specific electrical resistivity.
The thermal conductivity displays changes with different annealing times. However, these differences only occur at temperatures above 1000 °C. The thermal conductivity of materials D185 and IT180 increases when annealed for 120 h. With consecutive heat treatments, thermal conductivity increases for all materials, while electrical resistivity decreases for materials D185 and D180. In particular, for material IT180, the thermal conductivity increases with further heat treatments.
The saturation magnetization does not show any significant changes with different annealing periods. With consecutive heat treatments the saturation magnetization changes in all materials. Similar to the thermal conductivity, the saturation magnetization for all materials increases with consecutive heat treatments.
The Young's modulus appears to improve with heat treatments at temperatures above 1100 °C for material IT180 in particular. With shorter annealing times, the increase occurs only at higher temperatures. Due to this significant improvement of the Young's modulus, this material should be further investigated. Similar to the thermal conductivity and the saturation magnetization, the Young's modulus also increases sligthly for all 4 materials with consecutive heat treatments.

The strain of material D180 is found to be higher at samples annealed at 1100 °C than for samples annealed at 1300 °C. The strain of material IT180 is highest in the as-sintered state and decreases with higher annealing temperatures. Fracture surfaces of both materials show delamination, ductile fractures (comb fractures) as well as brittle fractures, pores and sintered contacts. Since tensile tests were only executed at two different annealing times, further investigations at different temperatures can be done.

After many attempts, a way to produce non porous binder materials with 0, 10, 20 and 30 % tungsten content was found within this thesis. With hot extrusion and subsequent heat treatments, dense materials, with tungsten mostly dissolved in the binder, were obtained. Solely, in the material with 30 % tungsten content,

Die approbierte gedruckte Originalversion dieser Diplomarbeit ist an der TU Wien Bibliothek verfügbar
The approved original version of this thesis is available in print at TU Wien Bibliothek.
TU Bibliothek Your knowledge hub WIEN

a separate tungsten phase is visible in SEM and XRD.
After consecutive heat treatments, a new, third phase occurs which failed to be determined in XRD.
The specific electrical resistivity decreases for binder materials with consecutive heat treatments. Generally, the specific electrical resistivity increases with increasing tungsten content. In contrast to this, the thermal conductivity decreases with increasing tungsten content. While the thermal conductivity increases with gradual heat treatments for the binder material with 20 % tungsten content, it decreases for the material with 30 % tungsten content. The saturation magnetization, however, increases at binder materials with 20 and 30 % tungsten. It decreases with increasing tungsten content for binder materials of 0, 10 and 20 % tungsten and decreases for the material with 30 % tungsten.
Since the hot extruded binder material was limited in its size, only consecutive heat treatments could be performed. Perhaps further experiments with non-consecutive heat treatments would show more changes in properties.

With low-temperature measurements it could be shown, that the electrical conductivity is higher with increasing tungsten content and with increasing temperature. There is a huge gap of almost 100 $\mu Ohmcm$ between the electrical conductivity of the sample with 20 % and the sample with 30 %. The curve for Ni-30 W has its minimum in the low temperature region. Furthermore, it can be confirmed, that the RRR value decreases with increasing tungsten content. The thermal conductivity was calculated using the Wiedemann-Franz law and the measured electrical conductivity at room temperature, however, these calculated values do not match the thermal conductivity measured in this thesis. The comparison of the specific electrical resistivity of the absolute values measured at ambient temperature and the specific electrical resistivity of the hot extruded FeNi/-xW binder materials after dissolution heat treatment at 1250 °C for 72 h and precipitation heat treatment at 1300 °C, at 1000 °C and at 800 °C for 2 h each, exposes significant differences.
Further investigations could be carried out in the field of low-temperature measurements, where thermal conductivity could also be measured and then compared with electrical conductivity via the Wiedemann-Franz law.

Die approbierte gedruckte Originalversion dieser Diplomarbeit ist an der TU Wien Bibliothek verfügbar
The approved original version of this thesis is available in print at TU Wien Bibliothek.
TU Bibliothek Your knowledge hub WIEN

References

[1] PLANSEE SE. *Tungsten heavy alloys*. Web Page. URL: https://www.plansee.com/de/werkstoffe/w-mmc.html.

[2] Jiten Das, G Appa Rao, and SK Pabi. "Microstructure and mechanical properties of tungsten heavy alloys". In: *Materials Science and Engineering: A* 527.29-30 (2010), pp. 7841–7847. ISSN: 0921-5093.

[3] Stefan Marschnigg. "Influence of starting materials, trace and interstitial elements on the sintering behavior and the properties of tungsten heavy alloys". Dissertation. TU Wien. 2018.

[4] Rafael Cury et al. "Evolution of cobalt-free tungsten heavy alloys for kinetic energy penetrators". In: *Powder metallurgy* 56.5 (2013), pp. 347–350. ISSN: 0032-5899.

[5] Y Şahin. "Recent progress in processing of tungsten heavy alloys". In: *Journal of Powder Technology* 2014 (2014). ISSN: 2090-7710.

[6] W. D. Kingery. "Densification during Sintering in the Presence of a Liquid Phase. I. Theory". In: *Journal of Applied Physics* 30.3 (1959), pp. 301–306. DOI: 10.1063/1.1735155. URL: https://aip.scitation.org/doi/abs/10.1063/1.1735155.

[7] C. Edtmaier et al. *Influence of heat treatment conditions on magnetic, thermal and electrical properties of tungsten heavy alloys.* In Proceedings of the 20th International Conference on Refractory Metals and Hard Materials (p.14). 2022.

[8] Herbert Danninger et al. "Bruchgefüge und Festigkeit von Wolfram- Schwermetallen/Fracture Surfaces and Mechanical Properties of Tungsten Heavy Metals". In: *Practical Metallography* 20.2 (1983), pp. 64–73. ISSN: 2195-8599.

[9] Moriya Oyane, Susumu Shima, and Tsuyoshi Tabata. "Consideration of basic equations, and their application, in the forming of metal powders and porous metals". In: *Journal of mechanical working technology* 1.4 (1978), pp. 325–341. ISSN: 0378-3804.

[10] Hung-Kuk Oh and Jeong-Keun Lee. "A study of the extrusion of sintered porous metal". In: *Journal of Mechanical Working Technology* 11.1 (1985), pp. 53–69. ISSN: 0378-3804.

Die approbierte gedruckte Originalversion dieser Diplomarbeit ist an der TU Wien Bibliothek verfügbar
The approved original version of this thesis is available in print at TU Wien Bibliothek.
TU Bibliothek Your knowledge hub WIEN

[11] Jinxu Liu et al. “Effect of fibrous orientation on dynamic mechanical properties and susceptibility to adiabatic shear band of tungsten heavy alloy fabricated through hot-hydrostatic extrusion”. In: *Materials Science and Engineering: A* 487.1-2 (2008), pp. 235–242. ISSN: 0921-5093.

[12] Zhou Xiaoqing et al. “Self-sharpening behavior during ballistic impact of the tungsten heavy alloy rod penetrators processed by hot-hydrostatic extrusion and hot torsion”. In: *Materials Science and Engineering: A* 527.18-19 (2010), pp. 4881–4886. ISSN: 0921-5093.

[13] GV Chester and A Thellung. “The law of Wiedemann and Franz”. In: *Proceedings of the Physical Society* 77.5 (1961), p. 1005. ISSN: 0370-1328.

[14] DIN Deutsches INSTITUT FÜR NORMIERUNG E. V. “Testing of metallic materials - Tensile test pieces”. In: *DIN 50125:2016-12. Berlin* (December 2016).

[15] Harald Reschab. “Systematische Untersuchungen zur Lorenz-Zahl bei hochlegierten Stählen”. Thesis. Technische Universität Graz. 2011.

[16] Christian Edtmaier et al. “Thermophysical behaviour of diamond composites for diode laser heat sink applications at temperatures between 4K and ambient”. In: 46th International Conference on Environmental Systems, July 2016.

[17] N Stojanovic et al. “Thermal conductivity in metallic nanostructures at high temperature: Electrons, phonons, and the Wiedemann-Franz law”. In: *Physical Review B* 82.7 (2010), p. 075418.

[18] Michael Schwarz. “Wärmeleitfähigkeit supraleitender Kompositleiter im Temperaturbereich von 4 K bis 300 K”. Dissertation. Universität (TH) Karlsruhe. 2009.

[19] Christian Edtmaier et al. “Temperature dependence of the thermal boundary conductance in Ag–3Si/diamond composites”. In: *Diamond and Related Materials* 57 (2015), pp. 37–42. ISSN: 0925-9635.

[20] Friedrich Kneidinger. “Non-centrosymmetric superconductivity of intermetallic compounds in absence of strong correlations among electrons”. Dissertation. Technische Universität Wien. 2014.

[21] Lin Hu, Brian D Wirth, and Dimitrios Maroudas. “Thermal conductivity of tungsten: Effects of plasma-related structural defects from molecular-dynamics simulations”. In: *Applied Physics Letters* 111.8 (2017), p. 081902. ISSN: 0003-6951.

Die approbierte gedruckte Originalversion dieser Diplomarbeit ist an der TU Wien Bibliothek verfügbar
The approved original version of this thesis is available in print at TU Wien Bibliothek.
TU Bibliothek Your knowledge hub WIEN

[22] Lei Lei Yang et al. "Evaluation on the interface characteristics, thermal conductivity, and annealing effect of a hot-forged Cu-Ti/diamond composite". In: *Journal of Materials Science Technology* 49 (2020), pp. 7–14. ISSN: 1005-0302. DOI: https://doi.org/10.1016/j.jmst.2020.02.023. URL: https://www.sciencedirect.com/science/article/pii/S1005030220302012.

[23] A. Fathy El-Kady and Omyma. "Thermal expansion and thermal conductivity characteristics of Cu–Al2O3 nanocomposites". In: *Materials Design (1980-2015)* 46 (2013), pp. 355–359. ISSN: 0261-3069. DOI: https://doi.org/10.1016/j.matdes.2012.10.042. URL: https://www.sciencedirect.com/science/article/pii/S0261306912007406.

[24] R Neu et al. "Investigations on tungsten heavy alloys for use as plasma facing material". In: *Fusion Engineering and Design* 124 (2017), pp. 450–454. ISSN: 0920-3796.

[25] U Ravi Kiran et al. "Effect of alloying addition and microstructural parameters on mechanical properties of 93% tungsten heavy alloys". In: *Materials Science and Engineering: A* 640 (2015), pp. 82–90. ISSN: 0921-5093.

Die approbierte gedruckte Originalversion dieser Diplomarbeit ist an der TU Wien Bibliothek verfügbar
The approved original version of this thesis is available in print at TU Wien Bibliothek.
TU Bibliothek Your knowledge hub WIEN

List of Figures

Die approbierte gedruckte Originalversion dieser Diplomarbeit ist an der TU Wien Bibliothek verfügbar
The approved original version of this thesis is available in print at TU Wien Bibliothek.
TU Bibliothek Your knowledge hub WIEN

Die approbierte gedruckte Originalversion dieser Diplomarbeit ist an der TU Wien Bibliothek verfügbar
The approved original version of this thesis is available in print at TU Wien Bibliothek.
TU Bibliothek Your knowledge hub WIEN

Die approbierte gedruckte Originalversion dieser Diplomarbeit ist an der TU Wien Bibliothek verfügbar
The approved original version of this thesis is available in print at TU Wien Bibliothek.
TU Bibliothek Your knowledge hub WIEN

Die approbierte gedruckte Originalversion dieser Diplomarbeit ist an der TU Wien Bibliothek verfügbar
The approved original version of this thesis is available in print at TU Wien Bibliothek.
TU Bibliothek Your knowledge hub WIEN

List of Tables

Die approbierte gedruckte Originalversion dieser Diplomarbeit ist an der TU Wien Bibliothek verfügbar
The approved original version of this thesis is available in print at TU Wien Bibliothek.
TU Bibliothek Your knowledge hub WIEN